UNIVERSITAT POLITÈCNICA
DE CATALUNYA
BARCELONATECH

PhD. Thesis
Design of Isofrequency Reconfigurable Repeaters

Author
Edgar Diaz Tapia

Thesis Advisor
Lluis Jofre Roca

A thesis sumited to the Universitat Politecnica de Catalunya (UPC) in partiall fulfillment of the requirements for the degree of
DOCTOR OF PHILOSOPHY
Barcelona, Octubre, 2013

Abstract

The advances in the communications systems has brought new requirements and challenges in terms of compactness and efficient systems that looking for increase the signal coverage area. The reconfigurable antennas are a promising solution for the communication systems when looking to improve the channel capacity and/or to extend the signal coverage. The main advantages of the reconfigurable antennas are the capabilities to change their frequency, polarization and radiation beam steering at a low cost. The reconfigurable antennas can be designed to operate in a determined changing environment keeping good electromagnetic characteristics. The design of reconfigurable RF repeaters is a relevant application of this reconfigurable antenna principle.

This thesis is devoted to study and propose new repeater architectures in which a set of reconfigurable parasitic elements as part of the repeater are used for reducing the electromagnetic coupling between the Rx and Tx antennas. It is shown that the use of the parasitic elements as a reconfigurable mechanism gives the flexibility to adapt the repeater electromagnetic characteristics to changing environments while keeping a good system performance. The determination of the minimum number of parasitic elements is an important parameter and it is determined by a modal analysis to define the minimum number of parasitic elements able to fulfill specific repeater electromagnetic characteristics. In order to validate the analytical results, different reconfigurable repeater prototypes controlled electronically are manufactured. A reconfigurable repeater prototype that is using eight reconfigurable parasitic elements has been designed for operating at different scatterer environments. The repeater reconfigurable capabilities are studied to evaluate the repeater performance in realistic indoor locations. Finally, in order to obtain a repeater with reconfigurable frequency isolation capabilities between the Rx and Tx antennas over a wide frequency range, a repeater prototype based on a pixeled layer as reconfigurable mechanism has been designed and measured.

Acknowledgments

Qusiera agradecer a mi padre Tomas Diaz y a mi madre Hortencia Tapia por estar siempre pendientes de mi a pesar de la distancia y el apoyo que me brindan en todo momento, a mis hermanos: Daniel, Olivia y Tomas y a mi primo Isai por todo el apoyo que me brindaron durante mi estancia en barcelona.

Tambien quiero expresar mi agradecimiento al Profesor Lluis Jofre por haberme aceptado como estudiante en AntennaLab y por haber dirigido esta tesis doctoral durante mi estancia en la UPC.

Un agradecimiento al Consejo Nacional de Ciencia y Tecnologia (CONACYT) de Mexico por la beca que me otorgo para realizar mis estudios de doctorado en la Universitat Politècnica de Catalunya durante estos años.

A mis colegas y amigos del grupo de investigacion AntennaLab: Eduardo Makhoul, Dani Rodrigo, Enrique Nova,Gemma Roqueta, Marta Guardiola, Maria Alonso, Marc Imbert, Jordi Balcells y Santiago Capdevila, quisiera agradecer todo el conocimiento que compartieron conmigo y en especial por la convivencia tan agradable que siempre me brindaron.

Al personal del TSC, a los tecnicos y secretarias un agradecimiento por el ambiente y trato amable que siempre me otorgaron.

Contents

Chapter 1

Introduction

The objective of this thesis work is to contribute to solve a problem that is often present in wireless communication systems: the lack communication coverage for a base station due the path propagation between a transmitting and receiving system. In the development of this thesis an isofrequency reconfigurable repeater model is presented and validated with an experimental isofrequency reconfigurable repeater controlled by electronic switches. First of all, the setting of the problem that motivates this thesis is identified, followed by the state of the art. Finally, the objectives and the organization of this thesis is presented.

1.1 Setting and definition of the problem

The modern wireless mobile systems are in continuous demand for improved coverage area and signal strength. However, the presence of scatterers and the signal attenuation between the transmitter and receiving systems reduces the coverage range of these systems. Actually the communication systems require coverage in difficult access locations like subways or in places where exist shadow areas that are uncover by the RF signal (Fig.1.1). A solution to enhance the RF coverage area is to use RF repeater devices. The RF repeater is a device that receives an RF signal with adequate level and retransmits it to a determined area where the signal is strongly attenuated or weak due the long distance between the transmitter and the receiving system. There are two kind of RF repeaters: passive and active. The passive repeaters not require amplifier stage in the RF signal while the active repeaters require an active RF amplifier stage [1–6]. Usually the passive repeaters are metallic reflectors that are placed in strategic places to reflect the incoming RF signal to shadow areas, but he main disadvantage of this repeaters is that the reflected signal is weak. The active repeaters are composed of a receiving and a transmitting antenna, in which the signal received in the Rx antenna is amplified by active elements like RF amplifiers and retransmitted by the Tx antenna. The coverage area of an active repeater depends on the gain of the active elements and the propagation losses.

An isofrequency repeater is a device in which the input and output signals are at the same frequency and a frequency conversion stage is not used. The main factor that limits the maximum gain of an active repeater is the electromagnetic coupling between the Rx antenna and the Tx antenna. In an isofrequency repeater, when the Rx and Tx antennas have low isolation between them, the electromagnetic feedback produces undesirable oscillations in the system. The isofrequency repeater has the advantage that the electronic circuitry control is simple, not require frequency conversion and the cost is reduced. The general block diagram of the isofrequency repeater is shown in Fig.1.2. Commonly in isofrequency repeaters a metallic plane is placed between the Rx and the Tx antenna for reducing the antenna mutual coupling.

A repeater can be designed to operate in indoor or outdoor locations. Interior private houses, buildings and closed places are examples of indoor locations, while urban areas, and open fields are examples of outdoor locations. In the outdoor locations the base stations require a high RF signal gain, for this reason when a repeater is used, it requires high isolation between the receiving Rx and transmitting Tx antenna. In the outdoor base stations

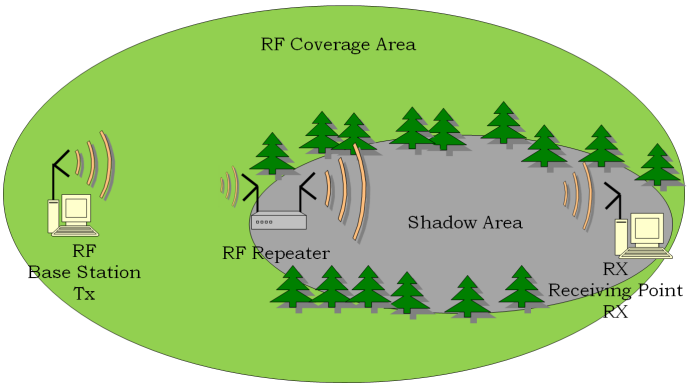

Figure 1.1 – General Repeater block.

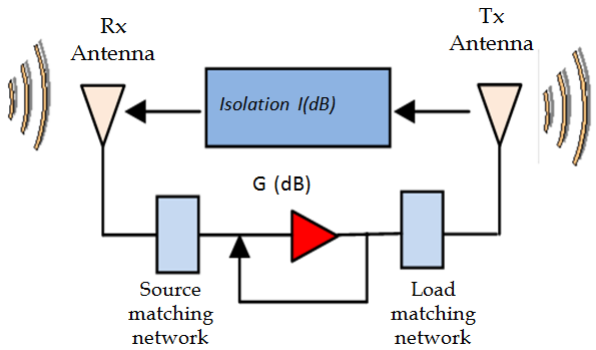

Figure 1.2 – General Isofrequency block.

increasing the RF power is an expensive solution because it increases the electromagnetic pollution. Using a repeater in indoor locations where there are a big number of scatterers that reflect the RF signal between the transmitting and the receiving system producing electromagnetic feedback, the isolation between the Rx-Tx antenna is reduced considerably, for this reason the repeater would require to be reconfigurable for enhancing and recover the isolation between Rx-Tx antenna in a changing scatterer environment. The required isolation in an isofrequency repeater in order to operate in a properly way is determined by:

$$I(dB) = G(dB) + S(dB) \tag{1.1}$$

where G is the amplifier RF gain and S is the safe margin to avoid undesirable oscillations and take values around 10-15 dB.

In the design of repeaters, the electromagnetic block isolator is the part that needs a special attention for obtaining a RF repeater device with good

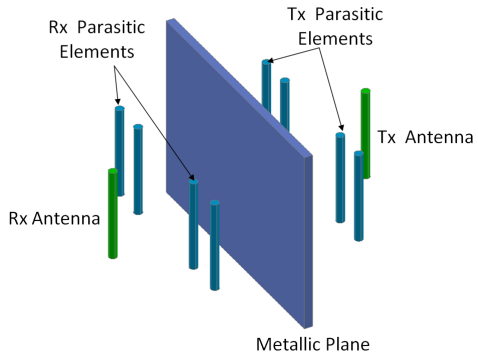

Figure 1.3 – Isofrequency repeater with a set of parasitic elements.

electromagnetic properties. The use of parasitic elements in multielement antennas is very common, specially when is required to have directive antennas with high gain, such is the case of the yagi-uda antennas, but nevertheless this is not the only application of the parasitic elements. The parasitic elements not only contribute to increase the bandwidth and the gain, but also can contribute to reduce the coupling between antennas. In different antenna references it has been reported that the coupling between two printed antennas is reduced around 40 dB using printed parasitic elements [7, 8]. The mutual coupling can be reduced as a function of the parasitic element position and length, and for different parasitic lengths, where the length is shifted until getting an optimum isolation value between two antennas. In resume, the isolation level between two antennas using parasitic elements depends on three factors: length, width and position of the parasitic elements. For this reason the study of the parasitic elements on antennas is an attractive topic because they present interesting properties in the modification of the antenna parameters. In the design of a repeater, the parasitic elements can be used in combination with a metallic plane for enhancing the isolation between the Rx and the Tx antenna, this geometry is shown in Fig.1.3. This thesis is focused in the study and development of isofrequency reconfigurable repeaters based on parasitic elements as a reconfigurable mechanism.

1.2 State of the art of repeaters

In the mobile commercial and private communications systems it is required to have a good as possible RF coverage. The isolation between the Rx and Tx antenna is an important parameter in active repeaters, and for this reason have been proposed different isolation techniques to be applied in the

design of repeaters [9–13], but in some of them the separation distance between the antennas is big, which is not useful when a compact repeater is required. In the following, different techniques to enhance the isolation between active elements are presented. A properly way to design a reconfigurable repeater capable to enhance, and recover the isolation between Rx-Tx antennas in a changing scatterer environment is also discussed.

The first step on the development of the repeater is to define the frequency range and the communication standard in which the repeater is designed to operate. The repeater has to be designed to operate under a promising communication standard, in this case was chosen WiMAX (Worldwide Interoperability for Microwave access) for the frequency band of north america due to the initial collaboration with the University of California at Irvine in this work. The WiMAX is a wireless communication standard designed to provide 30-40 megabit per second data rates. Actually, WiMAX is referred to interoperable implementations of the IEEE 802.16 family of wireless networks, and similarly WiFi refers to the interoperable implementations of IEEE 802.11 wireless LAN certified standard. Until now the designed WiMAX frequency bands are for : 2.40-2.48 GHz, 3.40-3.60 GHz, 4.50-4.90GHz, and 5.0-5.8GHz for licensed and unlicensed bands. For the case of indoor applications, the 5.0 GHz band has an advantage over the 2.4GHz frequency band, this is because is possible to get a wider bandwidth. The 5.0 GHz frequency band is an interesting band to design new wireless communication devices and specially to RF repeaters.The bands for 802.11a that operates in the frequency of 5.0GHz range are :

- Band A : Frequency range of 5.15-5.25 GHz with maximum EIRP (Effective Isotropically Radiated Power) of 50 mW used for indoor locations.
- Band B: Frequency range of 5.25-5.35 GHz with maximum EIRP of 250mW used for indoor and outdoor locations.
- Band C: Frequency range of 5.72-5.82GHz with maximum EIRP of 1W used for fixed service operations only.

1.2.1 Techniques to reduce the coupling between antennas

In a communication system where a multielement antennas is used, it exists a coupling effect and electromagnetic interference between antennas which is difficult to solve beyond a determined level using base band and processing signal techniques. The effects due to the undesirable antenna coupling are : system signal feedback, decoupling between the antenna and the amplifier,

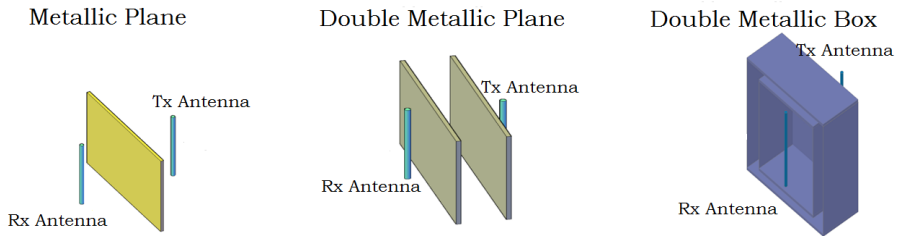

Figure 1.4 – Metallic plane shapes.

feedback in the amplifier, appearance of spurious signal levels and reduction in the transmit bit speed. In the next subsections some techniques to reduce the coupling between active antennas are mentioned.

1.2.1.1 Coupling reduction between antennas using metallic planes

The coupling between two antennas is strong when the electrical separation distance is short, in this case is common to use metallic planes to reduce the electromagnetic coupling [14]. Typically the active antenna is placed at $\lambda/4$ of the metallic plane with the finality to reduce the influence on the antenna impedance of the metallic plane and the electromagnetic coupling between two antennas. The metallic plane dimension has significant influence on increase the antenna isolation, getting up 20 dB for optimal metallic plane dimensions. For a particular case where there are two dipole antennas , the metallic reflector size to enhance the isolation is between $\lambda/2$ and λ and each dipole antenna is separated $\lambda/4$ from the metallic plane [15, 16]. In previous references the use of metallic reflectors has been proposed to increase the antenna isolation for different applications, it is the case of to use double metallic reflector in which the antenna isolation is around 45 dB. The use of metallic reflectors using double box is other option, but it is not always a good solution because the required space is big and the fabrication is expensive (Fig.1.4).

The use of metallic planes in the design of the isofrequency repeater is not enough because the isolation between antennas is a parameter that not only depends on the metallic plane shape but also depends on the scattering environment and the multiple electromagnetic reflections.

1.2.1.2 Coupling reduction between antennas using signal processing

There are computational signal processing techniques to reduce the coupling between antennas called coupling canceler or echo canceler [17, 18]. This technique has the function to reduce the electromagnetic coupling effects between two antennas estimating the phase, amplitude and the delay of the feedback signal. However, these systems are not able to control all the feedback signals under a variable time environment because the estimation of the phase, amplitude and the signal delay is not quite exact. The use of echo cancelers on the design of isofrequency RF repeaters is realized at intermediate frequency (IF) because the signal variation is slow and is more easily estimated. The computational complexity and the cost of the canceler technique on isofrequency repeaters is high and the device is limited to work at low rate, for this reason it is required to find other alternatives to design isofrequency repeaters with simple structure and working at higher signal rates.

1.2.2 Reconfigurable antennas

The reconfigurable concept when is referred to antennas, it means the capability to change the characteristic antenna electrical parameters through electric or mechanic mechanisms. Ideally, a reconfigurable antenna is designed to change the resonant frequency, input impedance, bandwidth, polarization, and radiation pattern as a function of the requirement systems [19–37]. There are different mechanisms in order to reconfigure the antenna characteristics:

- Electronic and Electromechanical switches: The effective parasitic length and consequently the resonant frequency can be shifted changing the antenna length placing switches over the antenna like PIN diodes, optical diodes, FETs and MEMS. Interesting switches are the MEMS, because they present low losses and high isolation.
- Variable loads: Different from the electronic and the electromechanical switches, the variable loads can change the antenna electrical length taking continue values (typically capacitive) on a determined range, and consequently changing the resonant frequency. The varactors are an example of the variable loads, and recently has been used integrated capacitors RF-MEMS to change the antenna patch resonant frequency [38].
- Structural mechanic changes: The antenna characteristics can be modified changing the antenna structure by mechanical systems [39].

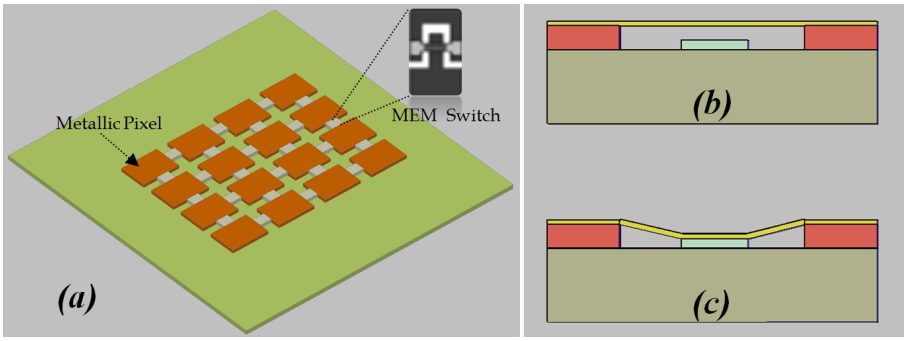

Figure 1.5 – a) Pixeled reconfigurable antenna structure. b) MEM switch "on" state. c) MEM switch "off" state.

- Material changes: The changes on the material characteristics in which the antenna is designed contribute to shift the antenna frequency, this permittivity material changes are used to modify the electrical antenna length.

In previous references it has been published experiments with pixeled reconfigurable antennas for designing MIMO systems. The pixeled reconfigurable antenna is based on the interconnection of a limited number of metallic pixels by MEMS-RF or PIN diodes over a laminated substrate for the design of microwave circuits Fig.1.5. The pixeled reconfigurable antenna is an attractive solution to get an antenna able to change its resonant frequency, polarization and the radiation pattern beam direction with the same structure.

There are many applications in which it can take advantage of the antenna capability to adjust its radiation pattern, the most common is the beam-scanning or beam steering. It consist of rotating automatically the antenna radiation pattern towards a certain interest direction or a determined base station, this is useful when there are mobile devices under line of sight (LOS) because high antenna gain can be obtained even when one or both communication systems are moving or rotating. The classical printed structures are using parasitic elements for getting radiation pattern reconfigurability (Fig.1.6).

1.2.3 Optimization Algorithms

The optimization algorithms are used in many engineering areas, because they help to find optimum numerical values that fulfill determinate cost functions. In the design of antennas the genetic algorithm (GA), particle

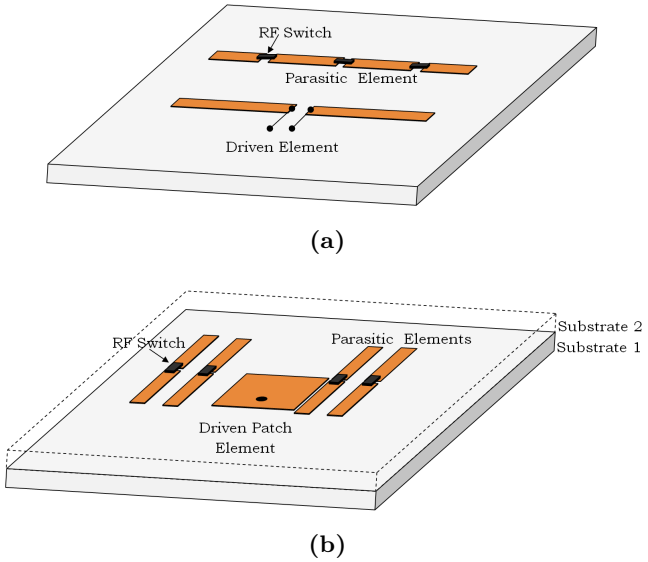

Figure 1.6 – Reconfigurable antennas using parasitic elements.

swarm optimization (PSO) and newton-rapson optimization are very useful to find optimal antenna dimensions and configurations in a determined multielement antenna [40–43]. In the case of pixeled reconfigurable antennas, the binary genetic algorithm (GA) is the most used to find an optimal code (determined number of switches in "ON" and "OFF" state) that cover specified parameters like impedance match, polarization, resonant frequency, etc. The PSO algorithm is used when it is required to adjust the antenna dimensions or the parasitic elements associated to the active antenna. In order to design an isofrequency reconfigurable repeater with specific electrical characteristics, the used optimization algorithm is the GA. The general GA flowchart is shown in Fig.1.7.

1.3 Objectives of the thesis

The encompassing objective of this doctoral work is to realize an isofrequency reconfigurable model based on the use of parasitic elements that helps to enhance the isolation between the Rx-Tx ports, optimizing the required number of parasitic elements for reducing the fields generated by a determined number of scatterers. The proposed model is validated by an isofrequency reconfigurable repeater prototype capable to enhance and recover high isolation level between the Rx and Tx ports in a real indoor

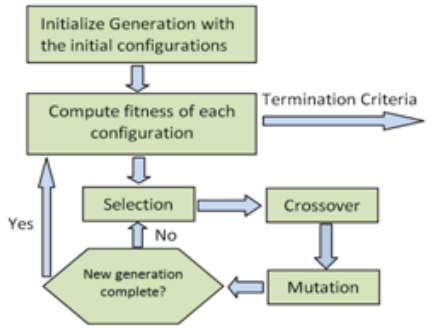

Figure 1.7 – Genetic Algorithm flowchart.

location. In order to obtain these goals, the research steps are divided as follows:

- To study, design and model an isofrequency repeater based on the spherical analysis able to obtain a modal decomposition of the electromagnetic field produced by a certain number of parasitic elements for their different configurations.
- To explore and to find a proper number of required parasitic elements to reduce and minimize the spherical wave coefficients generated by a determined number of scatterers that surrounds the repeater in order to design a low complexity reconfigurable repeater.
- To validate the isofrequency repeater model with a manufactured isofrequency reconfigurable repeater prototype controlled by electronic switches and exploring its reconfigurable capabilities in a real indoor location.
- To explore an alternative repeater able to support broader band isolation performances at the price of a higher complexity.

1.4 Outline of the document

This doctoral dissertation is organized in five chapters including this first chapter which exposes the setting of the problem, the state of the art and the main goals of this work.

- Chapter 2 addresses the analytical tools to compute the coupling between two antennas in free space and when a metallic plane reflector is

placed between them. The spherical wave expansion for the coupling between two antennas is presented as analytical tool in order to model an isofrequency repeater.

- Chapter 3 is focused on realize a repeater modeling and a modal study in the way in which the parasitic elements reduce the spherical wave coefficients generated by a determined number of scatterers. The first isofrequency reconfigurable repeater approximation is presented.
- Chapter 4 presents the experimental characterization of an isofrequency reconfigurable repeater based in the study realized in chapter 3. Also, an alternative reconfigurable repeater that has the capability to reconfigure the optimum isolation between Rx-Tx ports at different frequencies is presented.

The document is concluded with chapter 5 summarizing the main results presented along the presented work and commenting the future work.

Chapter 2

Antenna Mutual Coupling Analysis

The mutual coupling between antennas is the most important parameter in the design of the isofrequency repeaters because, as higher is the isolation between antennas, more free is the isofrequency repeater system of undesirable oscillations [44]. In order to obtain an optimum isofrequency reconfigurable repeater with high reconfigurable isolation capabilities between the Rx- Tx ports, it is required to know the existing coupling effects, exploring and proposing a way to reduce them. This chapter is devoted to review different analytical methods to compute the mutual coupling between two active antennas (dipoles in this case), introducing the spherical wave expansion as an useful analytical tool for the design of isofrequency repeaters. Two cases of mutual coupling analysis are considered, the first is when the antennas are in free space and the second case is when a metallic plane is placed between the two active antennas.

2.1 Coupling Between Antennas in Free Space

The receiving coupling voltage V_{Rx} is a measure of how much signal couples into the receiving antenna per unit input into the transmitting antenna, and in this section, different analytical methods to compute the receiving coupling voltage V_{Rx} in the Rx antenna when there are two active antennas (dipoles) are presented and compared with a modal method based on to decompose a field in a series of spherical wave coefficients, showing the advantages that this method presents in order to compute the mutual coupling at different antenna separations.

2.1.1 Far-Field coupling Approximation

The presented method is used to compute the mutual coupling impedance for the two antennas as a function of their effective length [45] and antenna separations larger than λ. Consider two dipoles separated a distance d_{ds}^{rt} as the presented in Fig.2.1, the mutual coupling impedance Z_{12}^{RT} for $d_{ds}^{rt} \gg \lambda$ can be computed as

$$Z_{12}^{RT} = jk\eta \frac{e^{-jkd_{ds}^{rt}}}{4\pi d_{ds}^{rt}} l_{ef}^{Rx} \cdot l_{ef}^{Tx} \tag{2.1}$$

where l_{ef}^{Rx} and l_{ef}^{Tx} are the effective length of the antennas (in this case referred as dipoles), η is the intrinsic impedance in vacuum and k is the wave number in the vacuum. Finally the ratio between the mutual impedance coupling and the mutual coupling voltage V_{Rx} is computed as $Z_{12}^{RT} = V_{Rx}/I_{Tx} \mid_{I_{Rx}=0}$, where I_{Rx} and I_{Tx} are the input currents into the Rx and Tx antennas respectively.

2.1.2 Induced EMF method

In an array of two elements, when the antennas are placed in a side by side configuration, with active dipole length in the Rx and Tx port defined as , the mutual coupling can be computed based in the induced EMF method presented in [46] for a distance separation between the Rx and Tx dipole d_{ds}^{rt} as

$$Z_{12}^{RT} = R_{12}^{RT} + X_{12}^{RT} \tag{2.2}$$

with

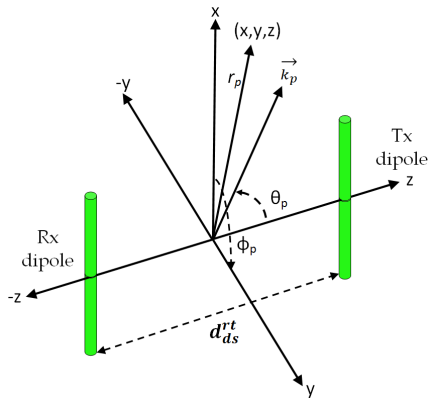

Figure 2.1 – Space Coordinate system to compute the antenna coupling.

$$\begin{aligned} R_{12}^{RT} &= \frac{\eta}{4\pi}[2C_i(u_o) - C_i(u_1) - C_i(u_2)] \\ X_{12}^{RT} &= -\frac{\eta}{4\pi}[2S_i(u_o) - S_i(u_1) - S_i(u_2)] \end{aligned} \tag{2.3}$$

and

$$\begin{aligned} u_o &= kd_{ds}^{rt} \\ u_1 &= k\sqrt{(d_{ds}^{rt})^2 + (l_{ad}^{Rx})^2} + l_{ad}^{Rx} \\ u_2 &= k\sqrt{(d_{ds}^{rt})^2 + (l_{ad}^{Rx})^2} - l_{ad}^{Rx} \end{aligned} \tag{2.4}$$

where S_i and C_i are the sine and cosine integrals which are defined in a general form as:

$$C_i(x) = \gamma + ln(x) + \int_0^x \frac{cos\tau}{\tau} d\tau \tag{2.5}$$

$$S_i(x) = \int_0^x \frac{sin\tau}{\tau} d\tau \tag{2.6}$$

with euler constant$\gamma = 0.577215664...$

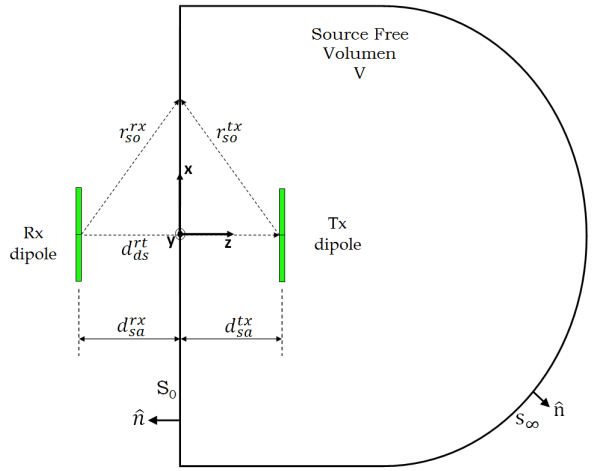

Figure 2.2 – Rx-dipole and Tx dipole reciprocity field geometry.

2.1.3 Lorentz reciprocity field

This analytical method has the advantage that the coupling between antennas can be computed by the cross product between the electric and magnetic field that produces each antenna over a plane at a determined distance and for a determined position. In order to compute the coupling between Rx-Tx antennas using the Lorentz reciprocity consider Fig.2.2. The source free volume V is bounded by the closed surface , consisting of the infinite plane surface S_o centered in the origin of the coordinate system and the surface at infinity S_∞. The Rx antenna placed at a distance d_{sa}^{rx} and the Tx antenna placed at a distance d_{sa}^{tx} produces the primary fields $\vec{E}^{Rx}$, $\vec{H}^{Rx}$ and $\vec{E}^{Tx}$, $\vec{H}^{Tx}$ over a plane surface S_o . The expression that relates the electric and magnetic fields generated by the primary sources to obtain the coupling voltage V_{Rx} [47] is defined by (2.7).

$$V_{Rx}(\vec{r_p}) = \int_{S_o} (\vec{E}^{Rx} \times \vec{H}^{Tx} - \vec{E}^{Tx} \times \vec{H}^{Rx}) \cdot \hat{n} ds \tag{2.7}$$

where $\vec{r}_p$ is the vector of relative position between the Rx and Tx antenna.

The expression (2.7) can be modified by expanding the primary fields in terms of their plane wave spectrum over the surface S_o. The plane wave spectrum can be determined analytically with the tangential fields $\vec{E}^{Rx}$ and $\vec{E}^{Tx}$ at every point in the plane.

$$\vec{E}^{Rx}\left(x,y,d_{sa}^{rx}\right)=\int_{-\infty}^{\infty}\int_{-\infty}^{\infty}\vec{F}^{Rx}\left(k_x,k_y\right)\cdot e^{-j\vec{k}_p\cdot\vec{r}_{so}^{\,rx}}dk_xdk_y \tag{2.8}$$

$$\vec{E}^{Tx}\left(x,y,d_{sa}^{tx}\right)=\int_{-\infty}^{\infty}\int_{-\infty}^{\infty}\vec{F}^{Tx}\left(k_x,k_y\right)\cdot e^{-j\vec{k}_p\cdot\vec{r}_{so}^{\,tx}}dk_xdk_y \tag{2.9}$$

in which the function $\vec{F}^{Rx}\left(k_x,k_y\right)$ is obtained from the tangential field components $\vec{E}_x^{Rx}$ and $\vec{E}_y^{Rx}$ as

$$F_x^{Rx}\left(\vec{k}_p\right)=\frac{e^{jk_zd_{sa}^{rx}}}{4\pi^2}\int_{-\infty}^{\infty}\int_{-\infty}^{\infty}E_x^{Rx}\left(x,y,d_{sa}^{rx}\right)\cdot e^{j(xk_x+yk_y)}dxdy$$

$$F_y^{Rx}\left(\vec{k}_p\right)=\frac{e^{jk_zd_{sa}^{rx}}}{4\pi^2}\int_{-\infty}^{\infty}\int_{-\infty}^{\infty}E_y^{Rx}\left(x,y,d_{sa}^{rx}\right)\cdot e^{j(xk_x+yk_y)}dxdy \tag{2.10}$$

The coupling tension in terms of plane wave spectrum can be obtained after a mathematical reductions [47],and considering $d_{sa}^{rx}=d_{sa}^{tx}$, the result expression is

$$V_{Rx}(\vec{r}_p)=\frac{8\pi^2}{\omega\mu}\int_{-\infty}^{\infty}\int_{-\infty}^{\infty}k_z\vec{F}^{Rx}\left(k_x,k_y\right)\cdot\vec{F}^{Tx}\left(k_x,-k_y\right)\cdot e^{-j\vec{k}_p\cdot\vec{r}_p}dk_xdk_y \tag{2.11}$$

2.1.4 Spherical wave expansion for the coupling coefficient

The spherical wave theory is a powerful tool that can be applied to analyze a wide range of antenna problems, especially an electromagnetic field, that in general can be expressed in terms of a series expansion, in which the expansion coefficients are defined by integrals over the source currents or boundary fields. When an integral formulation is used, the integral must be evaluated for each field point; instead with series formulation an integration is performed only once to determine the coefficients, and thereafter the series are summed for each field point [48–51].

The spherical wave expansion theory can be used to compute the mutual coupling voltage between two antennas because, (2.11) satisfies the scalar

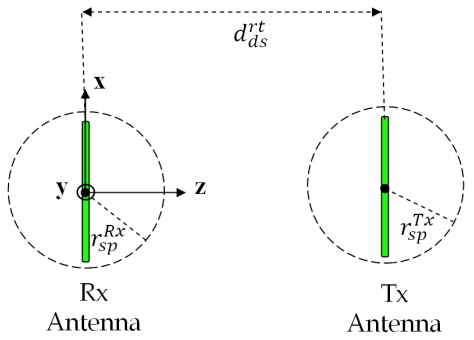

Figure 2.3 – Schematic of the Rx antenna and Tx antenna showing radius of each sphere surrounding the radiating portion of each antenna and oriented in a determined position in free space.

wave equation and thus can be expressed and expanded in a series of spherical waves [52] in order to compute the mutual coupling at different distances. The coefficients of the spherical waves may be obtained from the scalar product of the electric fields of the two antennas. Consider Fig.2.3, in order to compute the coupling tension in terms of spherical wave expansion, it is required to have the electric field that produces each antenna over a sphere that surrounds the main sources. The radii of the spheres that surrounds the Rx and Tx antennas are denoted by r_{sp}^{Rx} , and r_{sp}^{Tx}. The value of the coupling voltage can be computed as

$$V_{Rx}(\vec{r}_p) = \sum_{n=0}^{\infty} \sum_{m=-n}^{n} B_{nm} h_n^{(1)}(k d_{ds}^{rt}) P_n^m(\cos\theta_p) e^{jm\phi_p} \tag{2.12}$$

Where θ_p and ϕ_p are the spherical coordinate angles of the position vector $\vec{r}_p$ with respect to the coordinate system fixed in the Rx antenna, $h_n^{(1)}$ is the spherical hankel function of first kind, P_n^m are the associated legendre polynomials and B_{nm} are the spherical wave coefficients that change for each antenna pair and for each relative orientation of the antenna pair. The radii of the spheres r_{sp}^{Tx} and r_{sp}^{Rx} are important parameters because they determine the maximum number of modes required to evaluate (2.12).

For a specific case, (2.12) can be reduced since the interested direction of the antenna coupling is for $\theta_p = 0$ and $P_n^m(1)$ are non zero only for $m = 0$, (2.12) is then reduced to

$$V_{Rx}(\vec{r}_p) = \sum_{n=0}^{\infty} B_n h_n^{(1)}(k d_{ds}^{rt}) \tag{2.13}$$

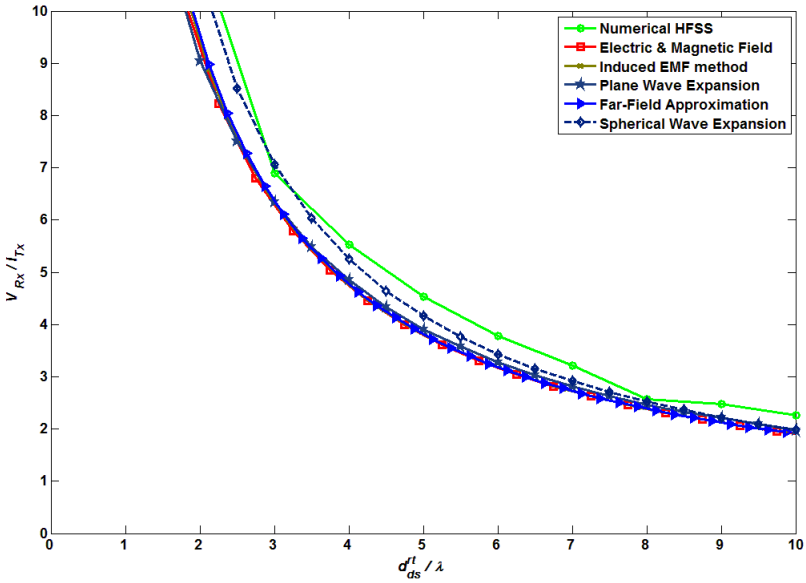

Figure 2.4 – Comparison of different analytical methods to compute the mutual coupling tension V_{Rx} between two dipoles in free space.

The coefficients B_{nm} are defined as

$$B_{nm} = \frac{j^n(2n+1)}{2}\frac{(n-m)!}{(n+m)!}\int_0^{\pi}\int_0^{2\pi} \vec{E}^{Rx}(\vec{r}_p)\cdot\vec{E}^{Tx}(-\vec{r}_p)\cdot P_n^m(\cos\theta_p)e^{-jm\phi_p}\sin\theta_p d\phi_p d\theta_p \quad (2.14)$$

and for the specific case of $m = 0$, (2.14) is written as

$$B_n = \frac{j^n(2n+1)}{2}\int_0^{\pi}\int_0^{2\pi} \vec{E}^{Rx}(\vec{r}_p)\cdot\vec{E}^{Tx}(-\vec{r}_p)\cdot P_n(\cos\theta_p)\cdot\sin\theta_p d\phi_p d\theta_p \quad (2.15)$$

Finally, the number of modes N required to compute the summation given in (2.12) and (2.13) is approximately

$$N \approx k_0(r_{sp}^{Rx} + r_{sp}^{Tx} + \lambda) \quad (2.16)$$

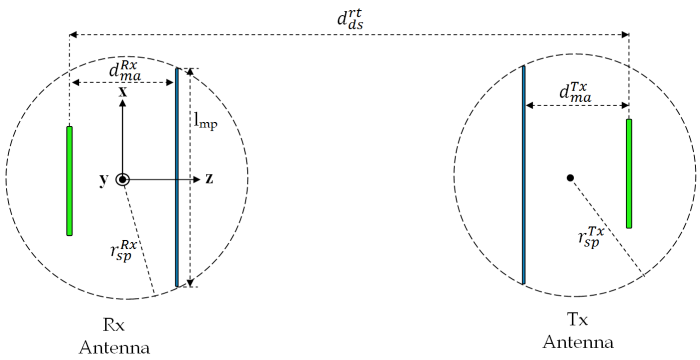

Figure 2.5 – Schematic of the Rx antenna and Tx antenna showing radius of each sphere surrounding the radiating portion of each antenna when is considered a metallic plane.

The different analytical methods presented in the previous sections used to compute the coupling voltage V_{Rx} for the side by side dipole orientation case are compared with the simulated results of a full-wave electromagnetic simulator (ansoft HFSS). This results are presented in Fig.2.4, in which it can be seen that the spherical wave expansion agrees with the numerical simulator results and with the different methods used to compute the mutual coupling voltage. The main advantage for using the spherical wave expansion is that the coupling voltage V_{Rx} between antennas can be computed once for one specific orientation and can be expanded at different distances, because the coupling B_n coefficients are unique, and has been assumed $e^{j\omega t}$ time dependence, and finally the outgoing waves use spherical hankel functions of first kind.

The information that the coefficients B_n gives, is useful because in the repeater analysis, if the coefficients B_n are reduced in magnitude or changed in phase by a determined mechanism, the coupling voltage between antennas is also changed because V_{Rx} is the sum of all created B_n coefficients.

2.2 Coupling between antennas in presence of a metallic plane

When a metallic plane reflector is introduced between two active antennas (dipoles), the Rx antenna and the Tx antenna each are considered inside a sphere of radii r_{sp}^{Rx} and r_{sp}^{Tx} that surrounds the Rx or Tx dipole plus the metallic plane as Fig.2.5. Due the to diffraction effects that are present when a metallic plane is introduced and in order to get more accurate results, the fields $\vec{E}^{Rx}(\vec{r}_p)$ and $\vec{E}^{Tx}(-\vec{r}_p)$ required to evaluate (2.14), are obtained with

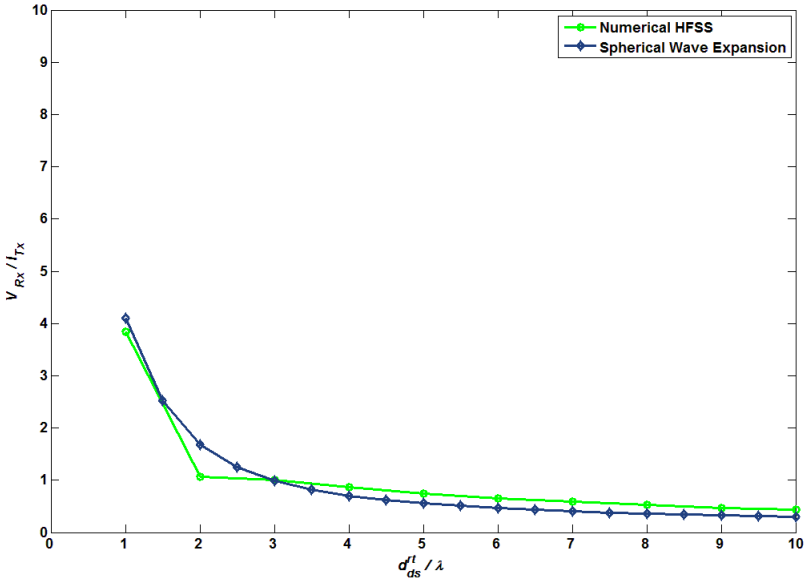

Figure 2.6 – Mutual coupling V_{Rx} computed when an $\lambda \times \lambda$ scatterer is placed between the Rx and Tx antenna.

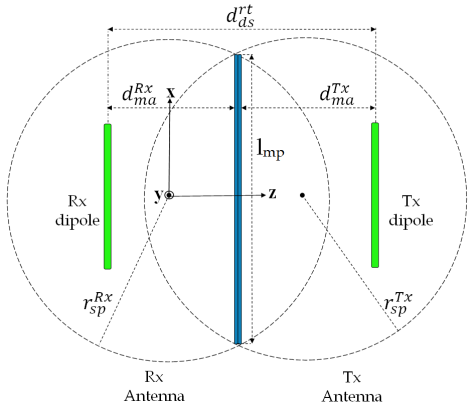

Figure 2.7 – Schematic of the Rx antenna and Tx antenna showing radius of each sphere surrounding the radiating portion of each antenna when is considered a metallic plane for $d_{ds}^{rt} = 0.92\lambda$.

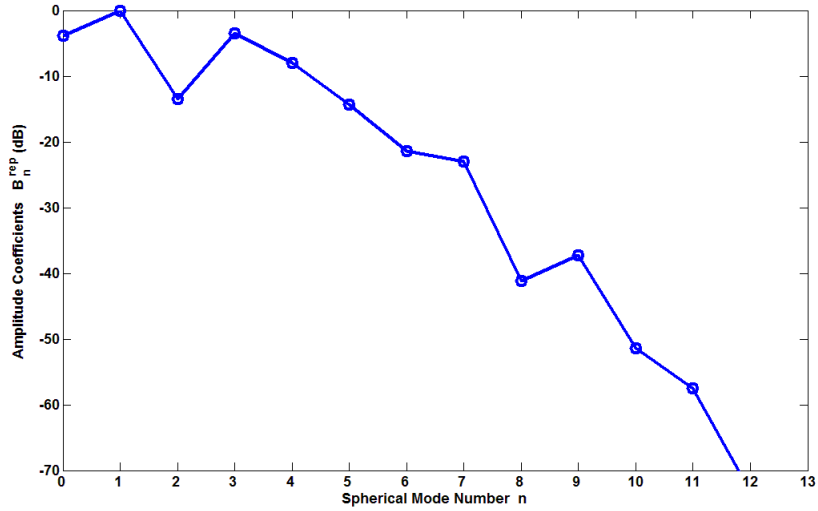

(a)

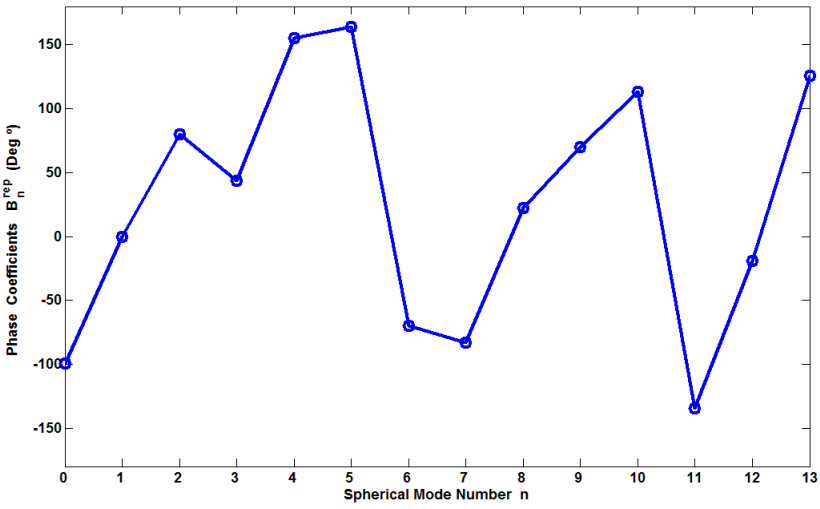

(b)

Figure 2.8 – Normalized amplitude and phase of the reference spherical wave coefficients B_n^{rep} (a) Amplitude. (b) Phase.

the full wave electromagnetic numerical simulator ansoft HFSS. In this case, is selected a $\lambda \times \lambda$ metallic plane because it is an optimum size to initialize the design of the repeater and this size keeps a good trade off between size and performance. The active Rx and Tx dipoles are placed at a distance of d_{ma}^{Rx} and d_{ma}^{Tx} from the metallic plane with dimensions of $l_{mp} \times l_{mp}$ in which $l_{mp} = \lambda$. The coupling voltage V_{Rx} as a function of the distance d_{ds}^{rt} and in presence of a metallic plane is computed first for a fix distance and then expanded to different distances using the spherical wave expansion. The modal computed coupling expansion for this case is computed and compared with the electromagnetic simulator results with good agreement as shown the Fig.2.6. The presented results shows that the coupling voltage can be evaluated for different antenna separation in an efficient way using the spherical wave expansion with the spherical coefficients computed with good accuracy.

As a fist step for the repeater modeling, the coupling spherical wave coefficients B_n are considered when is placed a metallic plane with dimensions of $\lambda \times \lambda$ mentioned before and for a fixed distance of $d_{ds}^{rt} = 0.92\lambda$ (Fig.2.7), in this case, the computed coefficients are named reference spherical wave coefficients B_n^{rep} for N=13. The normalized amplitude and phase of the reference coefficients are computed and presented in Fig.2.8.

2.3 Coupling With Parasitic Elements

In order to increase the reconfigurable capability of the repeater, a set of parasitic elements are added at both sides of the repeater. The parasitic elements interacts with the active elements in order to change the radiation pattern repeater properties depending the parasitic length and relative parasitic position from the active element.

The most simple case using parasitic elements is a geometry just with one active dipole element and one parasitic dipole element. In this case, when the active dipole has a length of $\lambda/2$ can be obtained three different radiation patterns which depends of the parasitic dipole length: 1) When is lightly longer, 2) equal and 3) lightly shorter (capacitive) than the active dipole. In the first case when the parasitic dipole is lightly longer (inductive) than the active element an electric field with its maximum in the direction of the active antenna, and for this reason is named reflector element, in the second case, when the parasitic element has the same length than the active element, the radiation pattern shape is almost symmetrical, and finally for the third case, when the parasitic length is lightly shorter than the active dipole an electric field with maximum in the parasitic direction is obtained, and is named director element. In order to visualize the effect

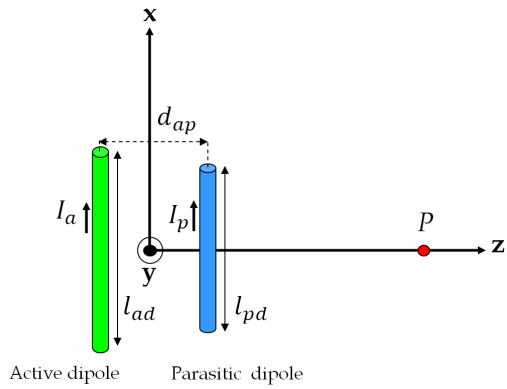

Figure 2.9 – Coordinate system of the active and parasitic element placed side by side to compute the total electric field in the point P.

that produces a parasitic element over the antenna field, consider Fig.2.9, the active element have a length of $l_{ad} = 0.45\lambda$ and the parasitic length l_{pd} is variable, the separation between the active and the parasitic element is $d_{ap} = \lambda/4$, which is the approximate distance between the active antennas and the parasitic elements in the proposed repeater model approached in the next chapter. The total electric field produced by the active element and the parasitic element is computed at the point P placed a distance of $\lambda/2$ from the parasitic element.

In order to compute the total field produced by the active element and the parasitic element in the point P :

$$\begin{aligned} V_{1a}^{ad} &= Z_{11}^{ad} I_a + Z_{12}^{pd} I_p \\ 0 &= Z_{21}^{pd} I_a + Z_{22}^{pd} I_p \end{aligned} \tag{2.17}$$

Where I_a is the current through the active element and I_p is the induced current by the active element over the parasitic element, V_{1a}^{ad} is the voltage in the active dipole. The induced current I_p and the input impedance in the active element due the interaction with the parasitic element Z_{in}^{ad} are obtained as

$$\begin{aligned} I_p &= \frac{-Z_{21}^{pd}}{Z_{22}^{pd}} I_a \\ Z_{in}^{ad} &= Z_{11}^{ad} + Z_{22}^{pd} \frac{I_p}{I_a} \end{aligned} \tag{2.18}$$

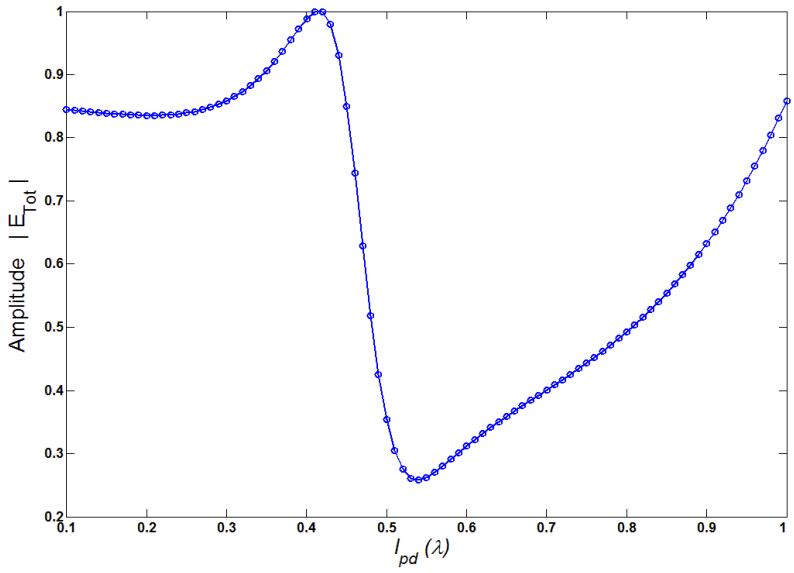

Figure 2.10 – Total field produced by the antenna (active plus parasitic element) P (0, 0, $\lambda/2$).

The total electric field $\vec{E}_{Tot}$ of a multielement antenna consisting of i elements is given by the sum of the electric field of the elements individually where the currents are represented by complex numbers and the phase differences in all directions are taken into account. The total electric field can be written

$$\vec{E}_{Tot} = \sum_{i=1}^{K} E\left(I_i\right) \tag{2.19}$$

where $E\left(I_i\right)$ is the electric field of the ith element carrying current I_i. With this consideration, the total electric field produced by the active element and the parasitic element in the point P is computed and in the Fig.2.10 is presented the normalized total electric field when the parasitic length l_{pd} changes.

Chapter 3

Repeater Modeling And Design

When two active antennas are separated by a metallic plane, the mutual coupling between them is reduced considerably, however the isolation generated by the metallic plane between the two antennas is not enough for the isofrequency repeater isolation requirements. In an indoor environment where there are a big number of scatterers that may change their position constantly, the isolation between the Rx and Tx changes also. In order, to solve this problem, the use of parasitic reconfigurable elements on the repeater design is a good alternative because when they are configured in a proper way, it is possible to enhance and to recover a high isolation between the Rx and Tx ports at the designed frequency even in presence of scatterers. The number of the parasitic elements used to reconfigure the electric repeater characteristics is an important parameter that needs to be defined because, using a high number of parasitic elements increase the cost and the repeater reconfiguration time. This chapter is devoted to model and design an isofrequency repeater based on a modal and a parametric study with the objective of knowing the required number of parasitic elements that needs to be used in the isofrequency repeater to get an optimum isofrequency repeater with good electromagnetic characteristics and performance in an indoor place.

3.1 Repeater model and coupling spherical coefficients

The effect that produces the parasitic elements over the coupling spherical coefficients B_n^{rep} presented in (2.12) has to be explored in order to analyze the isofrequency repeater performance when surrounded by scatterers. The coupling spherical coefficients generated by the repeater in free space are reduced when the parasitic elements configured in an optimum position and length are used, but, when the repeater operates in a scatterer environment, this coupling spherical coefficients are changed also, this is, the scatterers produce coefficients that are added to the original repeater coefficients B_n^{rep} changing in this way the coupling between antennas. In the next sections the effects that produce the parasitic elements over the coupling spherical coefficients B_n^{rep} are explored when their length, position and separation is changed with the repeater located in free space, also the effects that produce to reconfigure the parasitic elements when are placed a determined number of scatterers around the repeater are studied.

3.1.1 Repeater coupling spherical wave coefficients in free space

In order to model the repeater when the parasitic elements are introduced, consider Fig.3.1. In this first approximation a total of four parasitic elements are used. The fields $\vec{E}^{Rx}$and $\vec{E}^{Tx}$ generated at the Rx and Tx antenna locations are the sum of the field generated by the active dipole, the scattered field produced by the metallic plane ($\vec{E}_{sm}^{Rx}$ and $\vec{E}_{sm}^{Tx}$) plus the field reradiated by the parasitic elements ($\vec{E}_{p1}^{Rx}$,$\vec{E}_{p2}^{Rx}$,$\vec{E}_{p1}^{Tx}$,$\vec{E}_{p2}^{Tx}$) over their respective spheres.

$$\vec{E}^{Rx} = \vec{E}_{ad}^{Rx} + \vec{E}_{p2}^{Rx} + \vec{E}_{p1}^{Rx} + \vec{E}_{sm}^{Rx}$$

$$\vec{E}^{Tx} = \vec{E}_{ad}^{Tx} + \vec{E}_{p2}^{Tx} + \vec{E}_{p1}^{Tx} + \vec{E}_{sm}^{Tx} \tag{3.1}$$

When the parasitic elements are introduced, they have to be configured in terms of an optimum length and position in order to enhance the isolation and reduce as much as possible the parameter V_{Rx} between the Rx and Tx antennas. In a modal way, the parasitic elements change the phase and magnitude of the B_n^{rep} reference coefficients in such a way that from (2.15), the total sum of all coefficients is reduced and consequently the value V_{Rx}. The coupling spherical wave coefficients generated in the repeater for a

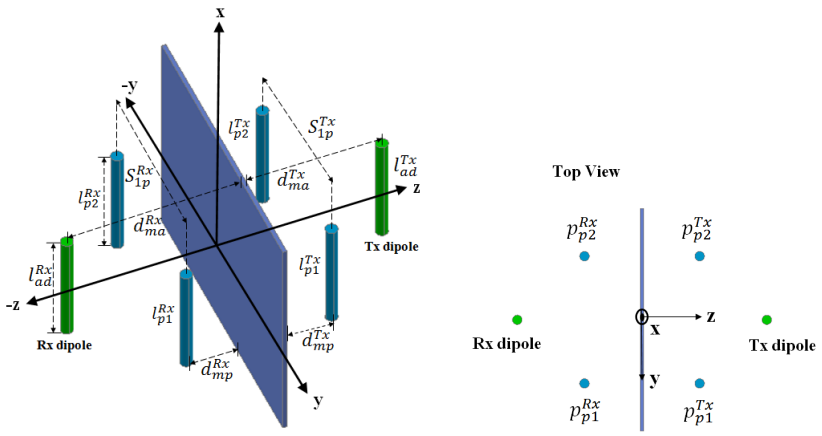

Figure 3.1 – Schematic of the isofrequency repeater using four parasitic elements.

certain number of parasitic elements are normalized with respect to the reference coupling spherical coefficients B_n^{rep} and are named repeater coupling spherical coefficients $B_n^{(rep,par)}$. In the Fig.3.2 the comparison between the coefficients B_n^{rep} with respect to $B_n^{(rep,par)}$ when the parasitic elements are introduced and configured in an optimum separation, position and length is shown. From this results, it is observed that the parasitic elements produce significant changes on the amplitude and phase of the B_n^{rep} coefficients.

3.1.2 Effect of the parasitic elements over the coupling spherical wave coefficients

In the repeater design, when the parasitic elements are introduced between the metallic plane reflector and the active antennas, it is required to explore the way in which the configuration of the parasitic elements modify the coefficients $B_n^{(rep,par)}$. In order to realize the mentioned study, we used as first approximation four parasitic elements considering symmetry between the Rx and Tx parasitic elements, this is d_{mp}= d_{mp}^{Tx}=d_{mp}^{Rx}, S_p=S_{1p}^{Tx}=S_{1p}^{Rx} and l_p=l_{p1}^{Rx}=l_{p2}^{Rx}=l_{p1}^{Tx}=l_{p2}^{Tx}, where the initial values are $S_p = 0.4\lambda$, d_{mp}=0.35λ, and l_p=0.66λ. In Fig.3.3, Fig.3.4 and Fig.3.5 the amplitude and phase for different values of d_{mp}, S_p and l_p are shown, where is observed that when the parasitic elements are moved along d_{mp} and when the length l_p is changed, they modify significantly the amplitude and phase of the $B_n^{(rep,par)}$ coefficients, and the parameter S_p have more influence over the change in phase of the coefficients $B_n^{(rep,par)}$. In order to modify the higher $B_n^{(rep,par)}$ modes, the parameter d_{mp} has to be increased, while the length l_p of the parasitic

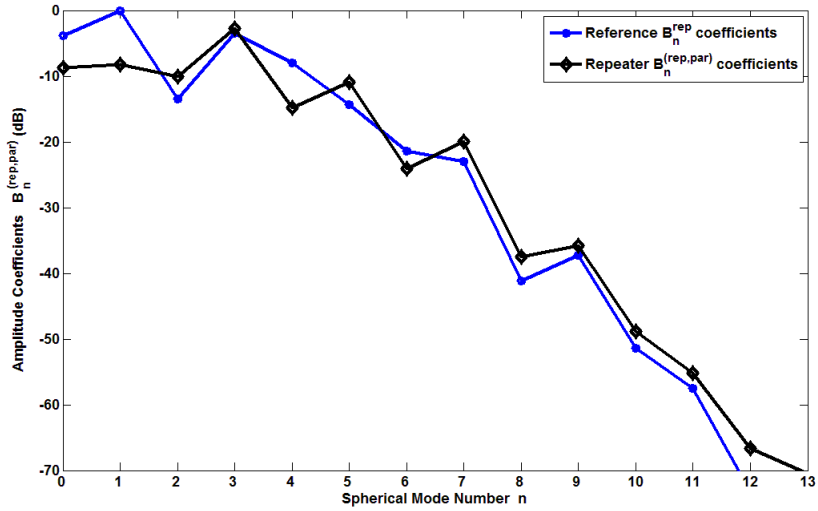

(a)

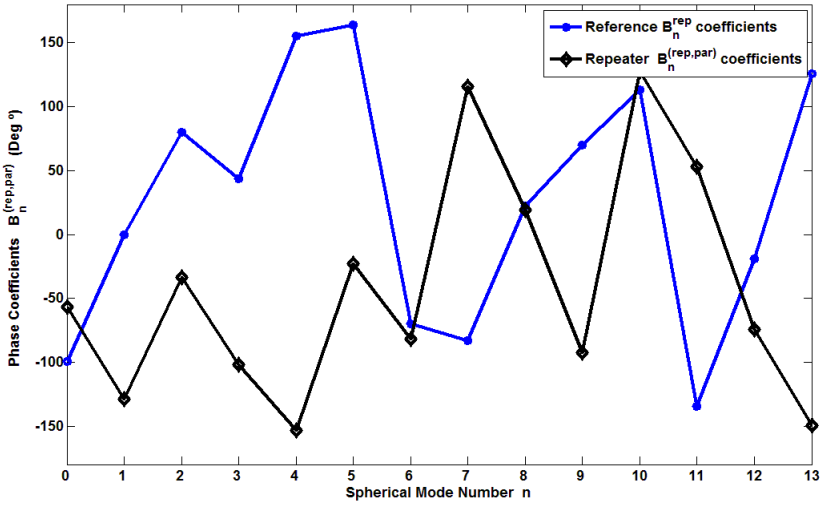

(b)

Figure 3.2 – Comparison between the coupling spherical coefficients B_n^{rep} and $B_n^{(rep,par)}$ in free space. (a) Amplitude (b) Phase.

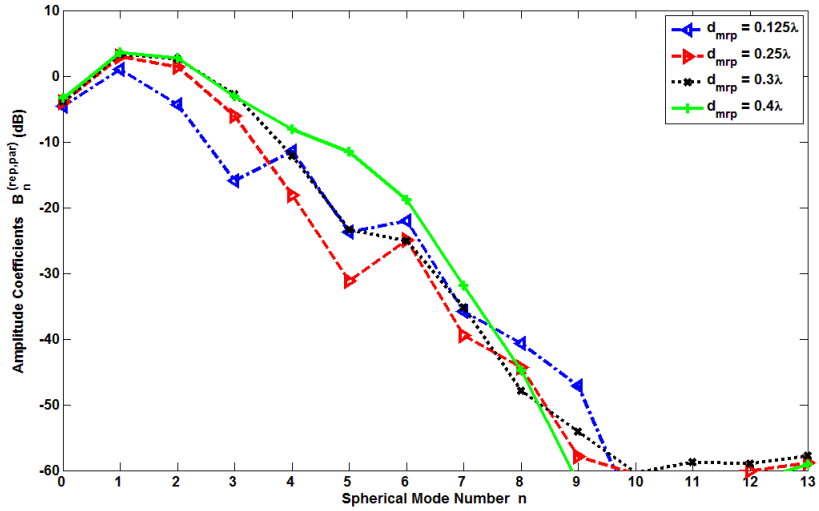

(a)

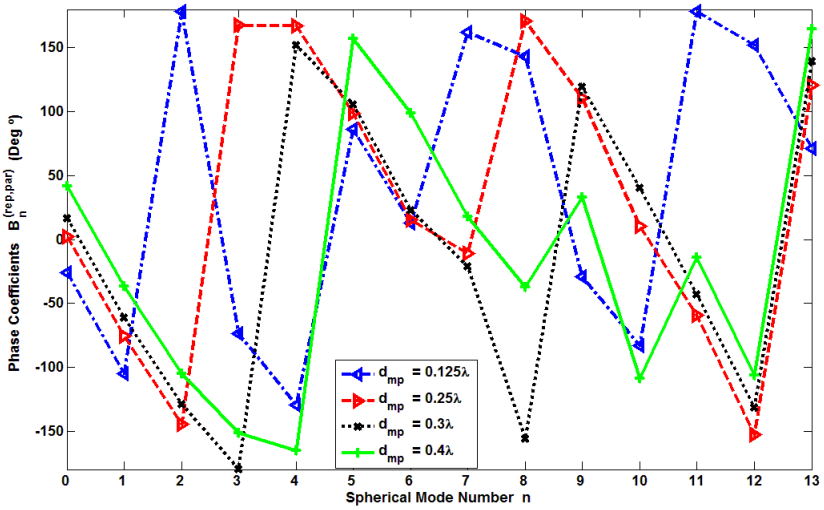

(b)

Figure 3.3 – Coupling spherical wave coefficients (a) amplitude (b) phase for different d_{mp} positions: 0.125λ, 0.25λ,0.3λ and 0.4λ.

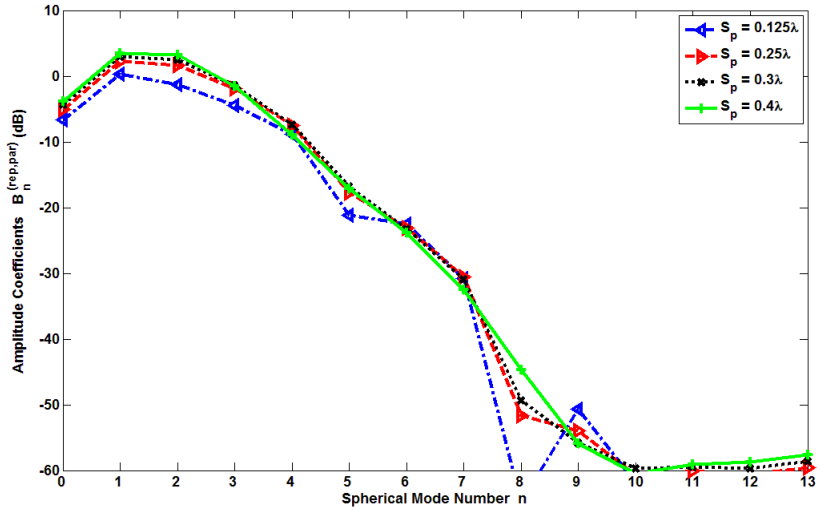

(a)

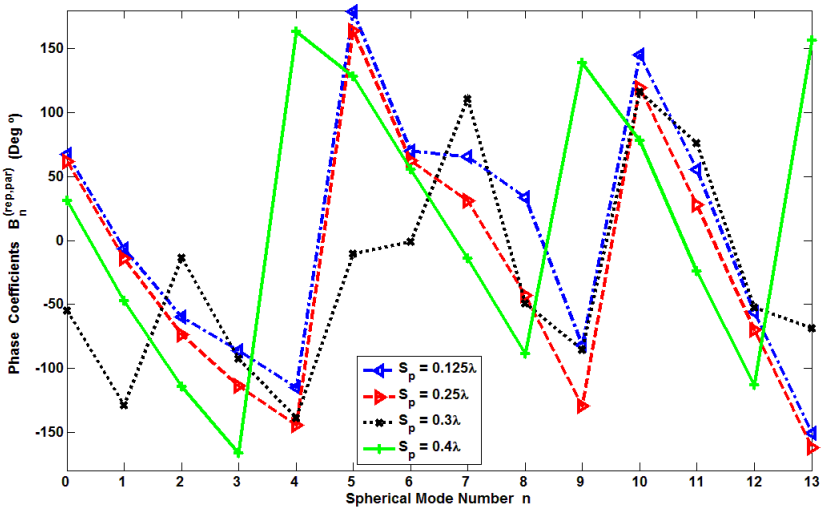

(b)

Figure 3.4 – Coupling spherical wave coefficients (a) amplitude (b) phase for different S_p positions: 0.125λ, 0.25λ,0.3λ and 0.4λ.

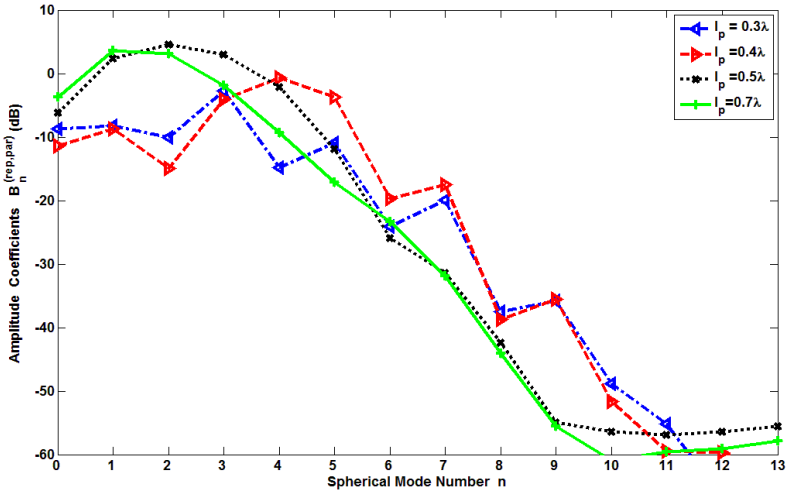

(a)

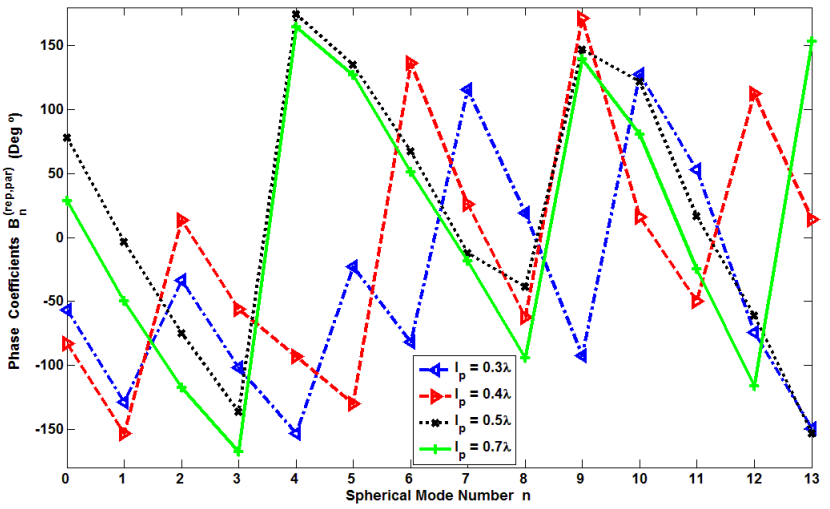

(b)

Figure 3.5 – Coupling spherical wave coefficients (a) amplitude (b) phase for different l_p positions: 0.3λ, 0.4λ,0.5λ and 0.7λ.

elements have to be short to modify the low order $B_n^{(rep,par)}$ coefficients and large to modify the high order $B_n^{(rep,par)}$ coefficients. When the parasitic elements are reconfigured in order to modify undesirable coupling spherical coefficients, is required to have an equilibrium in the configuration, this is, large parasitic elements that change the high coefficients order and short parasitic elements to modify the low coefficients order, in such a way that, the sum of all coefficients keep a low V_{Rx} value.

3.1.3 Repeater coupling spherical wave coefficients on a scatterer environment

When the isofrequency repeater is located in a scatterer environment, it is required to determine its reconfigurable performance, for this reason the repeater model has to be evaluated as a function of its capability to reduce, change and compensate the effects of the scatterers in terms of spherical modes as a function of the number of parasitic elements that are used, the number of scatterers and the distance in which the scatterers are placed from the repeater. In order to model the repeater in a scatterer environment, the field reflected by the scatterers is added to the field $\vec{E}^{Tx}$generated by the repeater. When a determined number of Si scatterers are placed in a random position, the field $\vec{E}^{Tx}$defined in (3.1) is now defined as

$$\vec{E}^{Tx} = \vec{E}_{ad}^{Tx} + \vec{E}_{p2}^{Tx} + \vec{E}_{p1}^{Tx} + \vec{E}_{sm}^{Tx} + \sum_{i=1}^{K} \vec{E}_{Si}^{Tx} \tag{3.2}$$

where $\vec{E}_{Si}^{Tx}$ represents the field generated by a determined Si scatterers over the Tx sphere of radii r_{sp}^{Tx}. The sphere that surrounds the Tx antenna has to include the Si scatterers, consequently as greater or distant are the scatterers, the radii r_{sp}^{Tx} is increased as the same way the N modes (see Fig.3.6). In order to explore the effect that the parasitic elements have in the modification of the $B_n^{(rep,par)}$ coefficients when scatterers are introduced, as a first step, two cases are considered, a) when a plane scatterer is introduced with dimension of $\lambda \times \lambda$ in a position $\vec{r}_{S1}^{Tx}(r_{S1}^{Tx} = 2\lambda, \theta_{S1} = 45^o, \phi_{S1} = 90^o)$ and (Fig.3.7 a), and b) when two plane scatterers are introduced with dimension $\lambda \times \lambda$ each and placed at $\vec{r}_{S1}^{Tx}(r_{S1}^{Tx} = 5\lambda, \theta_{S1} = 45^o, \phi_{S1} = 90^o)$ and $\vec{r}_{S2}^{Tx}(r_{S2}^{Tx} = 5\lambda, \theta_{S2} = 0^o, \phi_{S2} = 90^o)$ like the Fig.3.7 b. In both cases, when the parasitic elements are reconfigured in an optimum configuration, the $B_n^{(rep,par)}$ coefficients are changed, in such a way that the amplitude and phase of a determined region in the n modes map is affected more than other n mode map region. The reconfigured $B_n^{(rep,par)}$ coefficients for the case a) are presented in Fig.3.8 and for case b) are shown in Fig.3.9. From

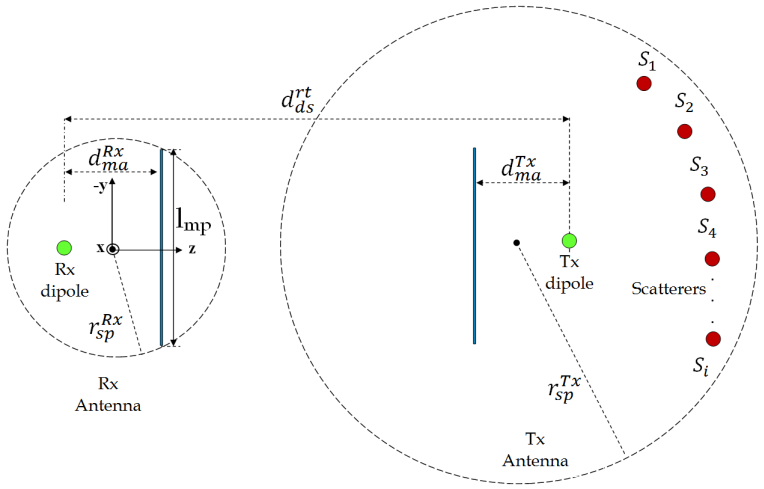

Figure 3.6 – Schematic of the Rx antenna and Tx antenna showing radius of each sphere surrounding the radiating portion of each antenna when is considered a metallic plane and scatterers.

the Fig.3.8 and the Fig.3.9 it may be observed that the proper configuration in the parasitic elements helps to change and reduce the n modes, however, for each scatterer position and size, the $B_n^{(rep,par)}$ is changing constantly, for this reason the parasitic elements needs high capability in reconfiguration for to compensate the n modes generated by the scatterers.

3.1.4 Repeater coupling spherical wave coefficients increasing the number of parasitic elements

In a scatterer environment, the repeater performance can change depending of the scatterer number, the scatterer size, and the distance from the metallic plane in which the scatterers are separated from the repeater. Depending on the number of parasitic elements that are used, the repeater reconfiguration capability and isolation between Rx-Tx ports can be enhanced. In order to validate this, a method to model a repeater with high reconfigurable capability, is considering big scatterers or scatterers placed in a position in which the reflections that they produce are high, in this way, if the parasitic elements can change and reduce the spherical wave coefficients generated by the scatterers in the mentioned case, then the repeater have high probabilities to compensate the spherical wave coefficients generated by small scatterers placed in a random position. In order to show how the parasitic elements number influence the $B_n^{(rep,par)}$ coefficients, a modal study is realized. Considering three metallic plane scatterers with dimension of $3\lambda \times 3\lambda$

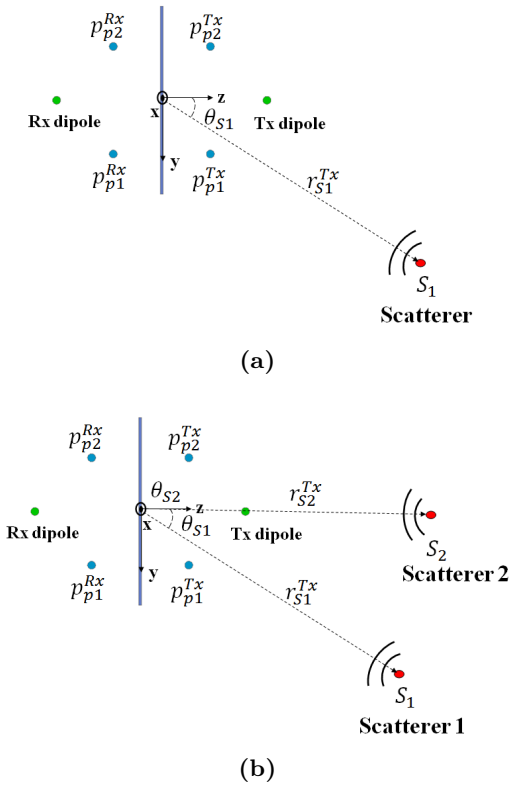

Figure 3.7 – Repeater model for one and two scatterers placed at (a) r_{S1}^{Tx}=2λ and (b) r_{S1}^{Tx}=5λ, r_{S2}^{Tx}=5λ.

are placed at a distance of $r_{S1}^{Tx} = r_{S2}^{Tx} = r_{S3}^{Tx} = 11\lambda$, at $\theta_{S1} = 45^o$, $\theta_{S2} = 0^o$ and $\theta_{S3} = -45^o$, thus different $B_n^{(rep,par)}$ coefficients are obtained using different number of parasitic elements, in this case a total of four, eight and twelve parasitic elements, and all reconfigured in an optimum configuration to compensate the coefficients generated by the three scatterers. In Fig.3.10 are presented a comparison of the reconfigured $B_n^{(rep,par)}$ coefficients magnitude and phase for 4, 8 and 12 parasitic elements in presence of the three scatterers. As can be observed in Fig.3.10, the $B_n^{(rep,par)}$ coefficients magnitude are reduced in a significant way when 8 parasitic elements are used in comparison to use 4 parasitic elements, however, when 12 parasitic elements are used the change of the $B_n^{(rep,par)}$ coefficients magnitude is similar than the case to use 8 parasitic elements.

In order to realize a study that links the number of necessary parasitic elements to reduce the coefficients $B_n^{(rep,par)}$ to the number of existing scatterers, a particular case is considered. The case consists in introducing a

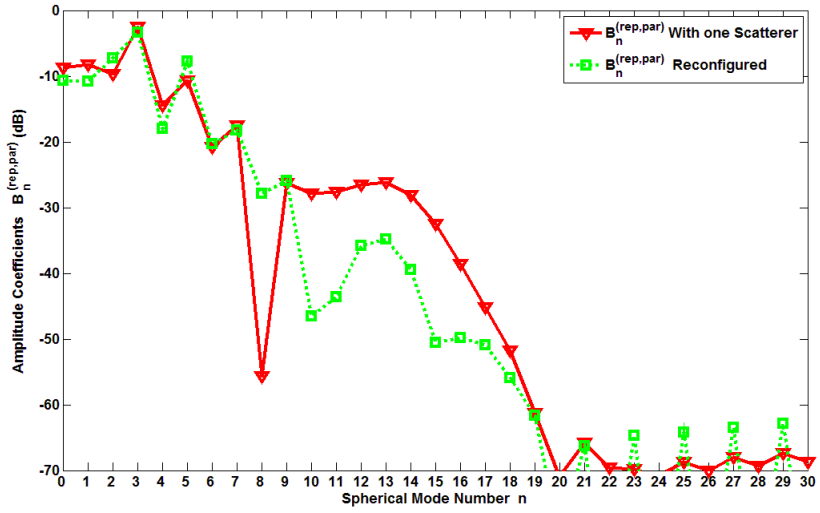

(a)

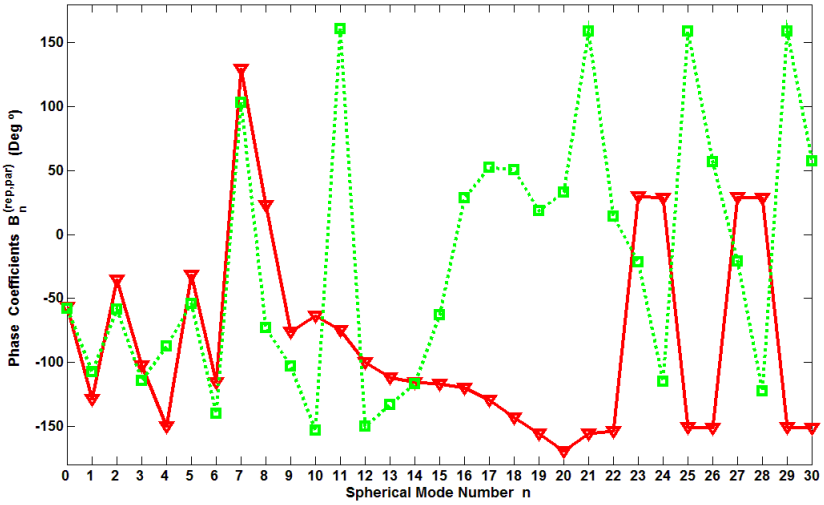

(b)

Figure 3.8 – $B_n^{(rep,par)}$ repeater normalized amplitude and phase coefficients for one scatterer placed at $r_{S1}^{Tx} = 2\lambda$with $\theta_{S1} = 45^o$.

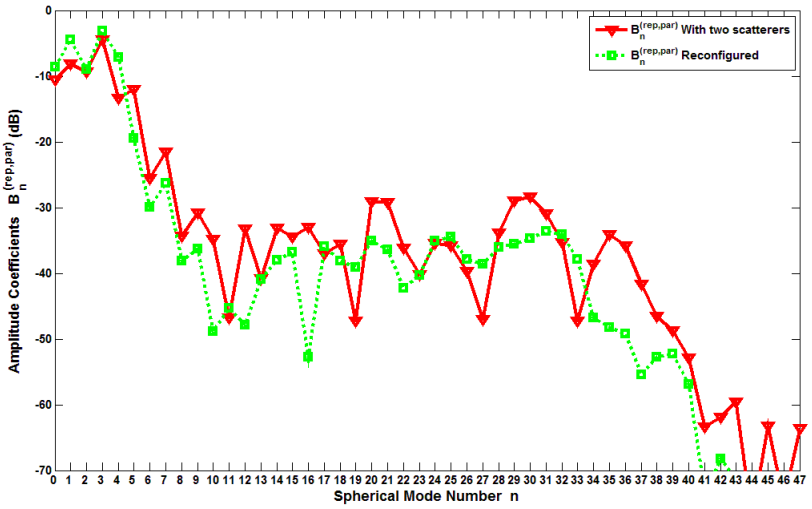

(a)

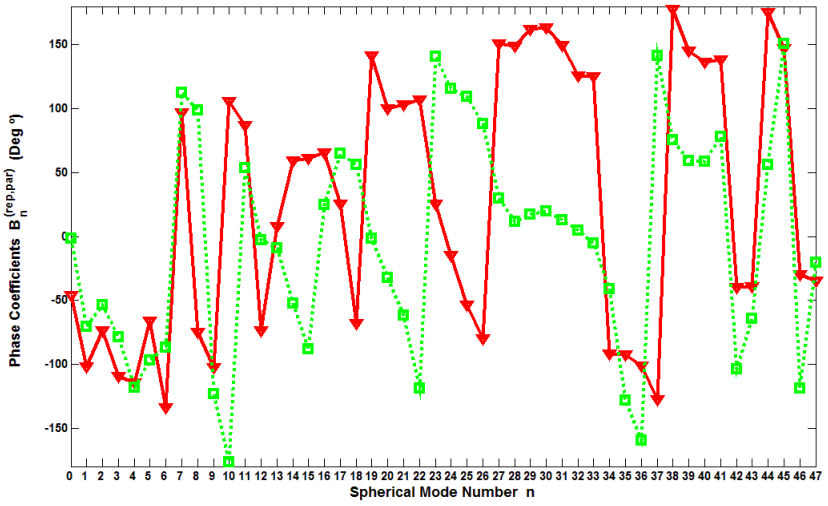

(b)

Figure 3.9 – $B_n^{(rep,par)}$ repeater normalized amplitude and phase coefficients for two scatterers placed at $r_{S1}^{Tx} = 5\lambda$, $r_{S2}^{Tx} = 5\lambda$, with $\theta_{S1} = 45^o$ and $\theta_{S2} = 0^o$.

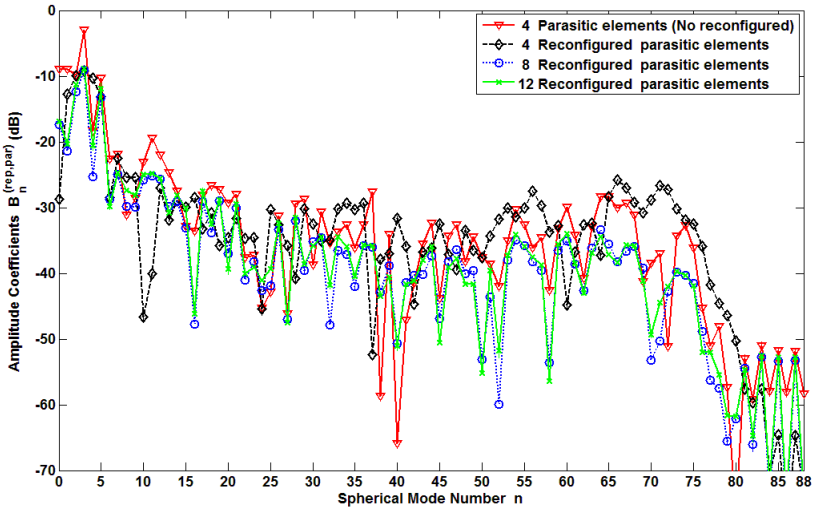

(a)

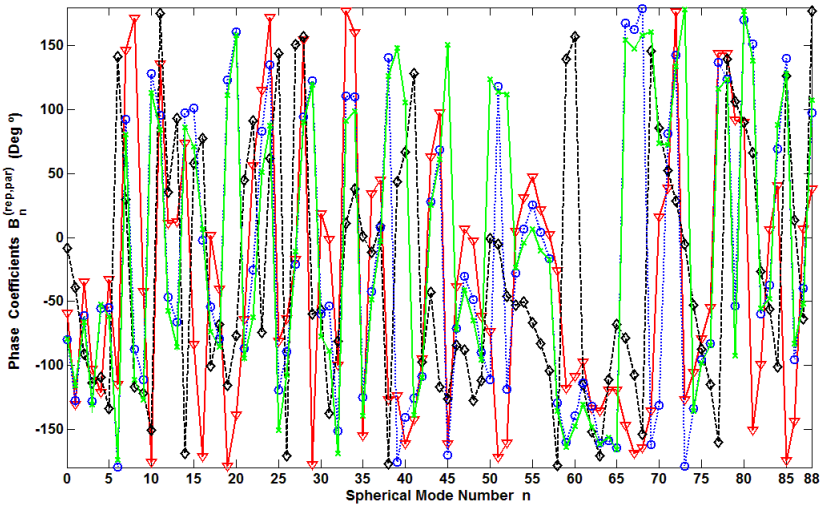

(b)

Figure 3.10 – Comparison of the $B_n^{(rep,par)}$ coefficients in presence of three scatterers and using 4, 8 and 12 reconfigurable parasitic elements.

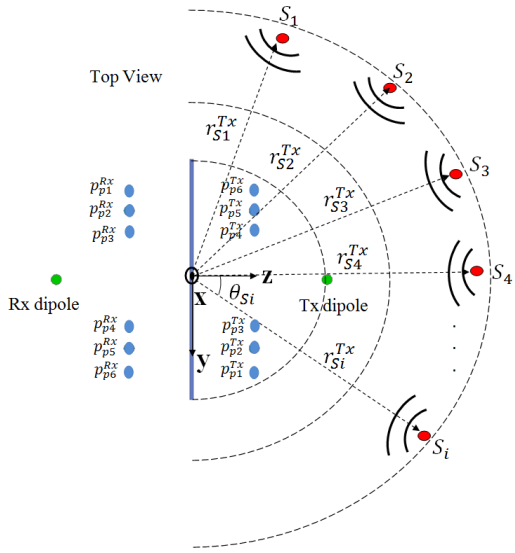

Figure 3.11 – Schematic of the isofrequency repeater model in presence of a determined Si scatterers using, 4 , 8 or 12 parasitic elements.

certain number of metallic plane scatterers with dimension of $3\lambda \times 3\lambda$ placed at different distances in positions that surrounds the repeater (Fig.3.11). In this case as mentioned before, metallic planes with dimension of $3\lambda \times 3\lambda$ are chosen because they produce strong reflections and is the proposed way to study the repeater reconfigurable capability in an indoor place. In Fig.3.12 are shown the results in a plot that links the number of parasitic elements required to reduce and compensated the spherical wave coefficients generated by a determined number of scatterers Si for this particular case (in this case metallic planes with dimension of $3\lambda \times 3\lambda$). From the Fig.3.12, with a total of 12 parasitic elements the repeater performance is good in comparison to use 8 and 4 parasitic elements, however the reconfiguration time that would require to use 12 parasitic elements is high. The required number to have a good trade off between the number of parasitic elements and the number of scatterers in which the repeater has still good performance are 8 parasitic elements. The presented results are taken as reference in order to design a repeater with high reconfigurable capabilities and low cost.

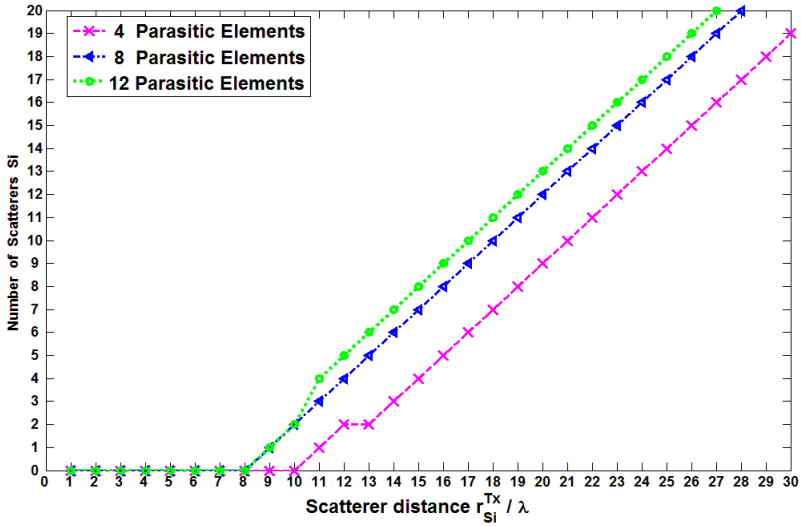

Figure 3.12 – Required number of parasitic elements for compensating a determined number of scatterers placed at different distances r_{Si}^{Tx}.

3.2 Design of the Isofrequency Reconfigurable Repeater

The influence of the parasitic elements over the spherical wave coefficients $B_n^{(rep,par)}$ and consequently over the parameter V_{Rx} in free space and when a certain number of scatterers are introduced, as seen in previous sections, has been studied. The parameter $Z_{12}^{RT} = V_{Rx}/I_{Tx}\,|_{I_{Rx}=0}$ is related directly to the scattering parameter S_{21}^{RT} by

$$S_{21}^{RT} = \frac{2Z_{12}^{RT}Z_0}{\Delta Z} \tag{3.3}$$

where $\Delta Z = (Z_{11}^{Rx} + Z_0)(Z_{22}^{Tx} + Z_0) - Z_{21}^{RT}Z_{12}^{RT}$.

From (2.13), related with the coefficients B_n^{rep} and, as mentioned, lower is V_{Rx}, from (3.3) lower is the scattering parameter S_{21}^{RT}. The high isolation between the Rx and Tx ports is obtained when pointing the Rx radiation pattern to a determined base station. Additionally a Tx wide radiation pattern are important characteristics that the repeater needs fulfill. There is a important trade off between the desired electromagnetic repeater characteristics and the repeater reconfigurable capabilities, for this reason, in the repeater design, genetic algorithms with a specific cost function that helps to find the best repeater configuration in a specific environment are used. In

order to validate the study presented in the last section a first isofrequency reconfigurable repeater is designed and manufactured.

3.2.1 Pixeled-Dipole Based Isofrequency Reconfigurable RF Repeater

The changes in position of scatterers surrounding an isofrequency repeater reduce the isolation level obtained with the initial configuration. In order to keep the Rx-Tx isolation level it is necessary to reconfigure and optimize the parasitic elements configuration. In particular: 1) to determine the position of the parasitic panel with respect the metallic reflector, 2) to determine the lateral separation between parasitic elements and 3) to determine the length of the parasitic elements.

In a real application, the length of the parasitic elements can be changed dynamically using pixeled lines interconnected with switches like MEMS or PIN diodes. These switching devices may be activated or deactivated to change the effective electrical length of the parasitic elements to make them act as strip director or reflector elements.

As first step an isofrequency repeater using 4 parasitic elements is designed to operate at 5GHz, showing that the reconfigurable dipole parasitic elements help improving the isolation level between the Rx and Tx ports in a dynamic way in presence of a nearby changing scatterer disposition by a reconfiguration of the parasitic dipole length. The shape of the Rx or Tx radiation pattern and so the isolation between the Tx and Rx ports of the repeater depends of the parasitic dipole length. For this reason, it is important to find a correct configuration of the parasitic elements to avoid electromagnetic coupling between ports.

In order to have high reconfiguration capability on the dipole parasitic elements, they can be substituted by a panel of reconfigurable parasitic strips interconnected by PIN diodes or MEMS, in this case a pixeled layer can be used, where the parasitic elements can be reconfigure changing their separation and length interconnecting the parasitic strips in a dynamic way (see Fig.3.13). As mentioned before, using a high number of switches the reconfiguration time is increased, however, the number of parasitic strips can be reduced drastically placing the strip parasitic elements in a sensitive position where the changes in the parasitic length modify in strong way the currents over the surface and consequently the radiated field.

In a first step the whole geometry was simulated using a full wave simulation and the genetic algorithm as global optimization tool. From the modal study realized in the section 3.1, and using the genetic algorithm, the optimization parameters are shown in the table 3.1. For fabrication and specially

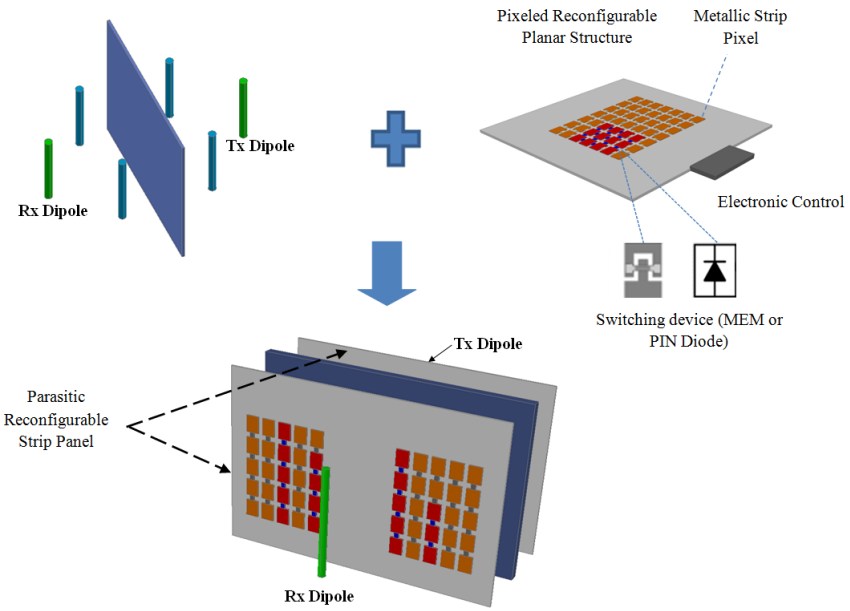

Figure 3.13 – Isofrequency reconfigurable repeater using a pixeled reconfigurable planar structure.

measurement simplicity, an isofrequency repeater version using monopole printed antennas is implemented, as shown in Fig.3.14. It consists of two sets of back to back monopole printed antennas fed by a coaxial probe. The active monopole has a length $l_{am}^{Rx} = l_{am}^{Rx} = 11mm$ and a separating on distance $d_{ma}^{Rx} = d_{ma}^{Rx} = 24.5mm$ from the metallic reflector. In order to improve the isolation level between the Rx and Tx ports, a parasitic panel with two pixeled strips separated a lateral distance $S_{1p}^{Rx} = S_{1p}^{Tx} = 34.4mm$ is placed at a distance $d_{mp}^{Rx} = d_{mp}^{Tx} = 10mm$ from the metallic ground reflector.The proposed prototype is referred as pixeled-dipole isofrequency reconfigurable RF repeater.

The distances $d_{ma}^{Rx} = d_{ma}^{Tx}$, $d_{mp}^{Rx} = d_{mp}^{Tx}$ and $S_{1p}^{Rx} = S_{1p}^{Tx}$ were optimized for the operating band 5GHz . The selected optimum distances were found to produce a maximum isolation level between the Rx and Tx ports maintaining good impedance matching. A study of the sensitivity with these different parameters showed that the length of the parasitic elements can change the frequency of maximum isolation between ports and recover the isolation level when is reduced due to a changing environment. As a result the only parameter that is changed with the optimization process is the pixeled upper parasitic lengths l_{up} that are added to a parasitic lower fixed lengths l_{lp}. In this design each metallic pixel strip has a width of $tp = 1.7mm$, and length

Repeater Optimization Process	
Initial Configuration	$d_{ma}^{Rx} = d_{ma}^{Tx} = \lambda/2$ $S_{1p}^{Rx} = S_{1p}^{Tx} = \lambda/2$ $d_{mp}^{Rx} = d_{mp}^{Tx} = \lambda/4$ $l_{p1}^{Rx} = l_{p2}^{Rx} = l_{p1}^{Tx} = l_{p2}^{Tx} = \lambda/4$
Restriction	$d_{ma}^{Rx}, d_{ma}^{Tx} \leq \lambda/2$ l_{lp} **with a fix value**
Optimization Parameters	$d_{ma}^{Rx} = d_{ma}^{Tx}$ $S_{1p}^{Rx} = S_{1p}^{Tx}$ $d_{mp}^{Rx} = d_{mp}^{Tx}$ l_{up}
Optimization Method	**Genetic Algorithm**
Criteria Goals	$min \left\lvert S_{21}^{RT} \right\rvert$ $min \left\lvert S_{12}^{RT} \right\rvert$ $min \left\lvert S_{11}^{Rx} \right\rvert$ $min \left\lvert S_{22}^{Tx} \right\rvert$

Table 3.1 – Pixeled dipole based Optimization isofrequency reconfigurable repeater parameters.

of 0.2 mm, being separated by a gap of 0.2 mm; therefore interconnecting an additional metallic pixel, discrete length increments of 0.4 mm in the overall parasitic length l_{up} can be achieved. Therefore the total effective parasitic length lines are $l_{p1}^{Rx} = l_{lp} + l_{up}$, $l_{p2}^{Rx} = l_{lp} + l_{up}$, $l_{p1}^{Tx} = l_{lp} + l_{up}$, $l_{p2}^{Tx} = l_{lp} + l_{up}$ where l_{lp} have a fix value of 4.4 mm, and l_{up} being of discrete variable length for each parasitic whole element. The width of the substrate and metallic ground reflector W_S is 60 mm, and their height h_S is 30 mm.

The parasitic elements help minimizing the back to back coupling in the Rx and Tx ports improving the isolation level between them. When the isolation level is reduced due to the presence of nearby obstacles, the parasitic element is reconfigured to a new optimum length. The parasitic length change produces a deviation in the angular direction of radiation reducing in this way the Rx-Tx coupling.

Microwave switches like RF-MEMS or PIN diodes may be used to interconnect the metallic pixels that change the length of the parasitic strips. In order to reduce cost for real applications the number of switches needs to be low. Additionally, an increase in the number of switches reduces the antenna efficiency and may increase the reconfiguration time. For simplicity and to demonstrate the practical effect of the pixeled parasitic lines on the

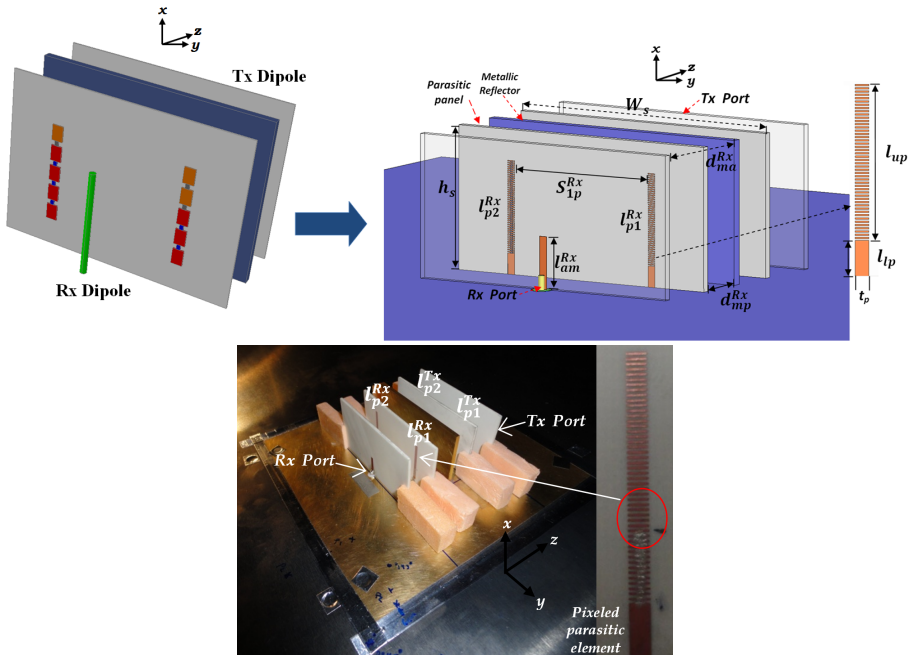

Figure 3.14 – Pixeled dipole based isofrequency RF repeater.

Total Parasitic length (mm)	l_{p1}^{Rx}	l_{p2}^{Rx}	l_{p1}^{Tx}	l_{p2}^{Tx}
Without presence of obstacle in the Tx port	10.8	10.8	10.8	10.8
With presence of lateral obstacle in the Tx port	16	10.8	11.2	14.8
With presence of obstacle rotated 45 in the Tx port	11.2	11.2	10.8	10.8

Table 3.2 – Optimum pixeled parasitic length.

isolation level, the length of the pixeled lines were reconfigured by short circuiting them with silver painting, emulating as a first approximation the state "*on*" and "off" of the switching devices.

To experimentally verify the simulated results, an isofrequency repeater prototype has been manufactured. The substrate used has been RO4003 (ε_r=3.55,$tan\delta$=0.0027) with a thickness of 1.52 mm. The prototype is shown in Fig.3.14. As commented by interconnecting the pixeled parasitic dipoles is possible to reconfigure each parasitic element to adopt certain length improving the isolation level for a determined environment. The optimum length of the parasitic elements obtained are shown in table 3.2.

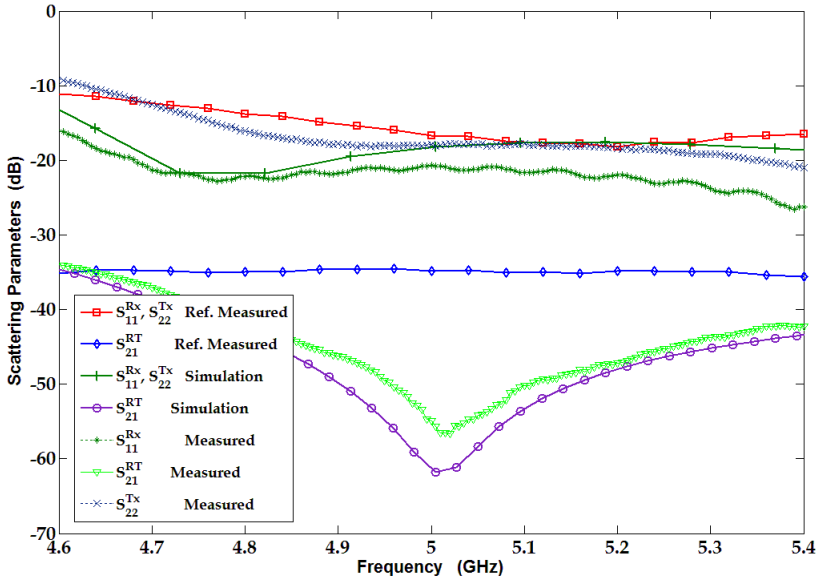

Figure 3.15 – Scattering parameters of the repeater optimized without obstacle presence.

The measured initial isolation reference level between the Rx and Tx ports separated by a metallic ground reflector (dimension of $\lambda \times \lambda/2$) at 5GHz and in absence of nearby scatterers and without parasitic elements is 35 dB, referred as reference isolation level. When a parasitic panel is placed at an optimum position ($d_{mp}^{Rx} = d_{mp}^{Tx}$) and the parasitic strip length are optimized, the isolation level may be improved 20 dB from the reference level while maintaining good impedance matching. The simulated and the measured scattering parameters are presented in Fig.3.15. The simulated radiation pattern in the Rx port and the Tx port of the repeater is similar when no obstacle is present, it can be observed in Fig.3.16.

In order to verify the reconfigurable capabilities of the proposed repeater an obstacle with two different geometries is located in the Tx coverage area: 1) The repeater is in presence of a 0.5λ x 0.5λ metallic plane scatterer, positioned in lateral position at 0.5λ from the Tx printed monopole edge. 2) The obstacle considered in case 1 is now rotated -45^o in the yz plane respect to the Tx printed monopole panel and separated 0.5λ from the edge.

In the case 1, when the obstacle is introduced, its isolation level between ports at 5GHz is first reduced to 47 dB from its previous 57 dB (optimized with no obstacle presence), but when the pixeled parasitic strips are recon-

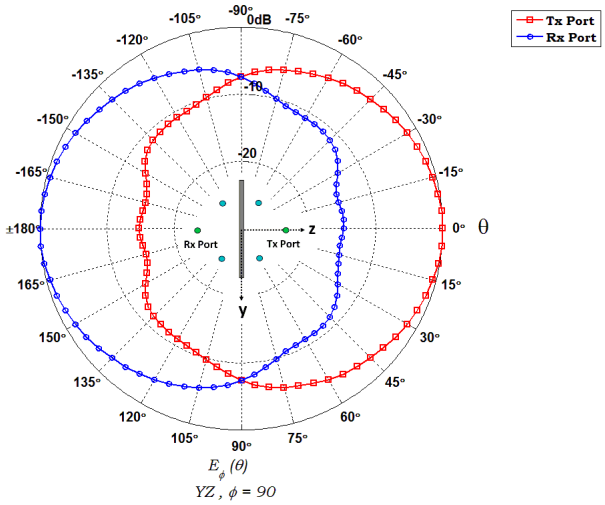

Figure 3.16 – Normalized radiation pattern of the pixeled-dipole repeater without presence of scatterer.

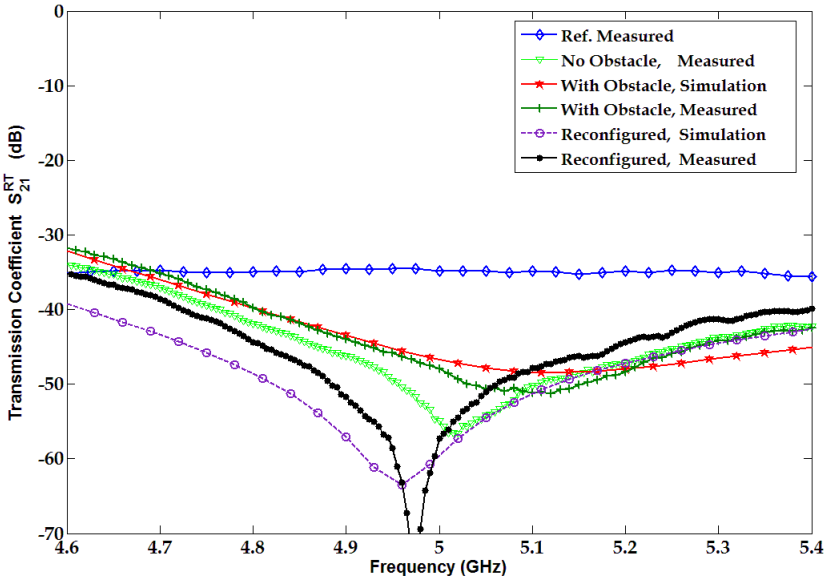

Figure 3.17 – Reconfigured S_{21}^{RT} parameter in presence of a lateral obstacle.

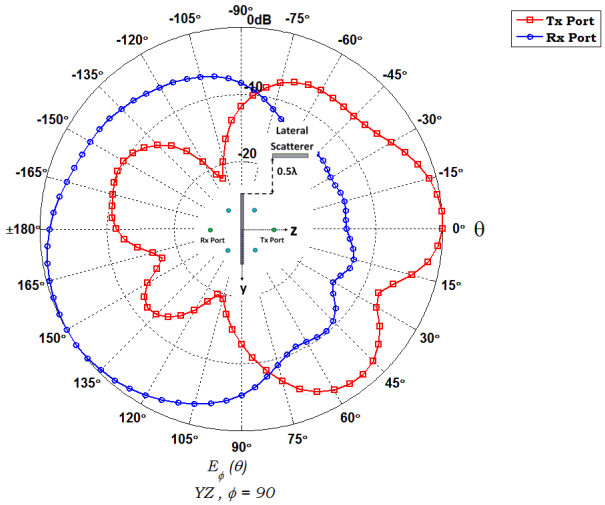

Figure 3.18 – Normalized reconfigured radiation pattern of the pixeled-dipole repeater with presence of a lateral scatterer.

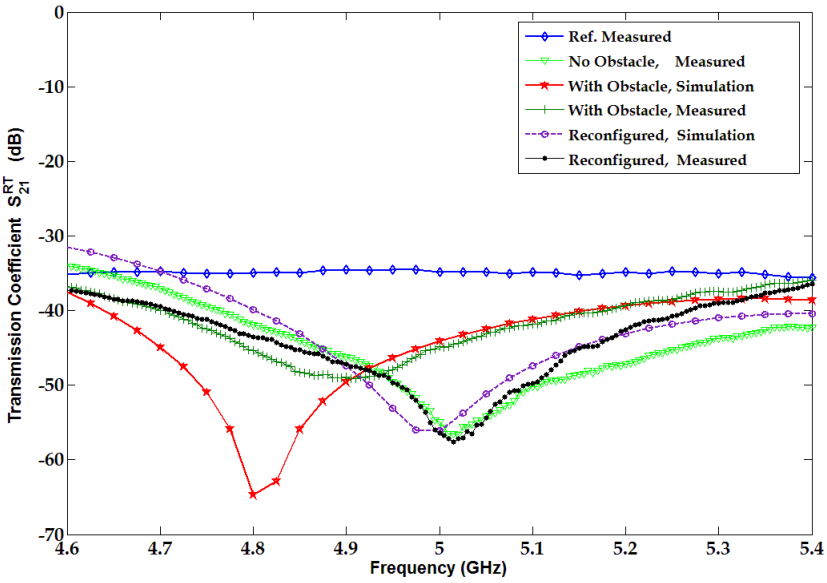

Figure 3.19 – Reconfigured S_{21}^{RT} parameter in presence of a -45 degrees position scatterer.

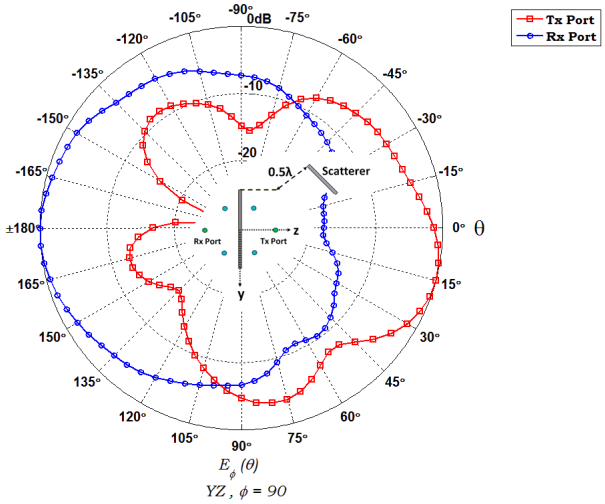

Figure 3.20 – Normalized reconfigured radiation pattern of the pixeled-dipole repeater with presence of a -45 degrees position scatterer.

figured for the new scenario, the isolation level goes back at 55 dB. It is important to mention that good impedance matching is also achieved. The genetic algorithm was used to find the optimum length of each pixeled parasitic strip. In Fig.3.17 it is shown that the simulated parameter S_{21}^{RT} agrees well with the measured results. In the Tx port of the repeater, the shape of the radiation pattern is deformed in presence of an scatterer, and when the repeater is reconfigured, the new parasitic configuration tries to deviate the angular direction of the radiation pattern. In Fig.3.18 the simulated radiation pattern in the repeater Rx and Tx ports is presented.

For the case 2, the isolation level at 5 GHz is reduced to 45 dB when the scatterer is present. When the parasitic strips are reconfigured to the new optimum length, the measured isolation level at 5GHz goes back to 55dB. In the Fig.3.19 is presented the simulated and measured S_{21}^{RT} parameter when the repeater is reconfigured.The corresponding simulated radiation pattern in the Rx and Tx port is shown in Fig.3.20.

Based in the modal study realized in this work, when the parasitic elements have a determined length, they have strong influence on the spherical wave coefficients and consequently reducing the tension coupling V_{Rx} at the designed frequency, however, for a fix active antenna length $l_{am}^{Rx} = l_{am}^{Rx} = 11mm$ and when the parasitic length change, the coupling voltage V_{Rx} change and can be optimum for other frequency where the main active antenna is well match. This property is important because the repeater not

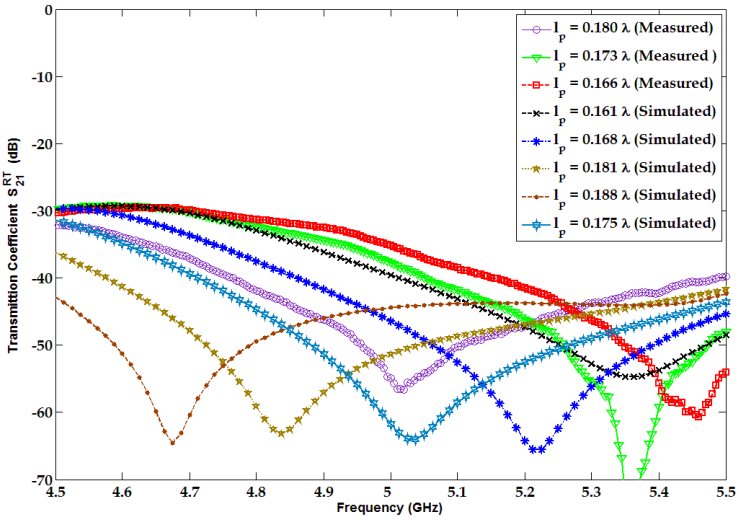

Figure 3.21 – S_{21}^{RT} Frequency reconfigurable repeater response in free space when the total parasitic length l_p is changed in a symmetrical way.

only can be reconfigured to recover the isolation level at the designed frequency when there are scatterers around the repeater, but also the repeater can be reconfigured to operate in other frequencies. In the Fig.3.21 simulated and measured S_{21}^{RT} parameters are presented when the reconfigurable repeater is in free space and the total parasitic length l_p is changed in a symmetrical way where can be observed that changes $\ll \lambda/30$ has strong influence on the repeater reconfiguration capability. This first prototype has paved the way for a real implementation of an isofrequency reconfigurable repeater.

Chapter 4

Isofrequency Reconfigurable Repeater Prototype

In the previous chapter it has been presented a modal analysis that shows the way in which the parasitic elements have a significant influence over the repeater performance. To validate it, a first reconfigurable repeater approximation has been built. For a realistic application, the required number of parasitic elements and switches in the repeater has to be low, because the reconfiguration time has to be short and able to keep a good repeater performance in an indoor location. An alternative to improve the isolation in a dynamic way consisting on reconfiguring the plane between the Tx and Rx elements. This can be obtained by using a pixeled layer that interconnects a determined number of strip pixels in a dynamic way. After presenting the optimization model process, the chapter follows presenting first an experimental isofrequency reconfigurable repeater prototype using eight parasitic elements and eight switches electronically controlled and producing high reconfigurable isolation and radiation pattern capabilities. In a second step a manufactured reconfigurable repeater prototype using a pixeled layer that can be reconfigured to enhance the isolation between the Rx-Tx ports over a wide frequency range is presented.

4.1 Port Optimization Loading Model

The optimization process in a reconfigurable antenna is an important design step, specially when is desirable to have a multifunctional antenna. The use of computational scripts and algorithms are the usual recurrence design tools, in which the genetic algorithms are the most used. When a pixeled reconfigurable antenna is designed with a determined number of pixels interconnected by M_{sw} switches and a determined number of feed active antennas N_{AA}, it is well know that depending on the environment and the electromagnetic antenna specifications, the pixel antenna switches state change [53–55]. To connect the genetic algorithm to the reconfigurable antenna, and get the best antenna switch configuration that fulfill the electromagnetic antenna specifications, a full-wave simulation of the geometry problem is developed using the finite element method electromagnetic solver Ansoft (HFSS). In the simulation, each one of the operational switches is replaced by lumped ports and in this way only a single full simulation is realized to evaluated the $2^{M_{SW}}$ possible configurations. The number of configurations is the result of the number of switch elements that can be in ON or OFF state. From the simulation data, the scattering parameter matrix S is exported and this matrix has dimension of $N_P \times N_P$, where N_P is the total number of used ports.

The network model representation of the pixeled antenna is depicted in Fig.4.1 where, a_1 and b_1 represent the incident and reflected waves in the feeding coaxial cable of the active ports, a_2 and b_2 represent the incident and reflected waves on each of the M_{sw} switches distributed across the pixeled panel. The matrix S can be obtained from the simulator as:

$$S = \begin{pmatrix} S_{11}^{N_{AA}\times N_{AA}} & S_{12}^{N_{AA}\times M_{SW}} \\ S_{21}^{M_{SW}\times N_{AA}} & S_{22}^{M_{SW}\times M_{SW}} \end{pmatrix} \tag{4.1}$$

and

$$\begin{bmatrix} b_1 \\ b_2 \end{bmatrix} = \begin{bmatrix} S_{11}^{N_{AA}\times N_{AA}} & S_{12}^{N_{AA}\times M_{SW}} \\ S_{21}^{M_{SW}\times N_{AA}} & S_{22}^{M_{SW}\times M_{SW}} \end{bmatrix} \begin{bmatrix} a_1 \\ a_2 \end{bmatrix} \tag{4.2}$$

with

$$a_2 = \Gamma_R b_2, \qquad \Gamma_I = \frac{b_1}{a_1} \tag{4.3}$$

combining the (4.2) and (4.3) :

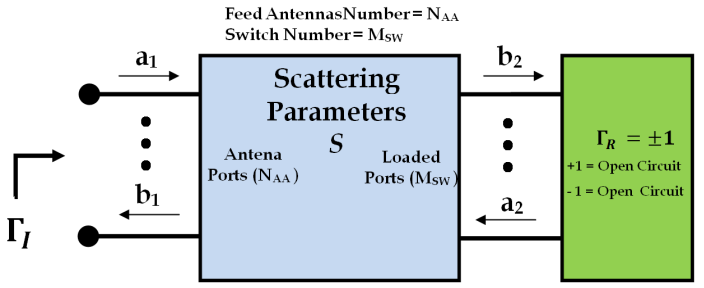

Figure 4.1 – Network model representation of a pixeled antenna.

$$b_1 = S_{11}^{N_{AA}\times N_{AA}} a_1 + S_{12}^{N_{AA}\times M_{SW}} \left(I^{M_{SW}\times M_{SW}} - \Gamma_R S_{22}^{M_{SW}\times M_{SW}}\right) \Gamma_R S_{21}^{M_{SW}\times N_{AA}} a_1 \quad (4.4)$$

and the total antenna scattering parameters Γ_I are extracted as

$$\Gamma_I = S_{11}^{N_{AA}\times N_{AA}} + S_{12}^{N_{AA}\times M_{SW}} \left(I^{M_{SW}\times M_{SW}} - \Gamma_R S_{22}^{M_{SW}\times M_{SW}}\right) \Gamma_R S_{21}^{M_{SW}\times N_{AA}} \quad (4.5)$$

where Γ_R is a identity matrix in which the diagonal elements can take the value of 1 or -1, if $\Gamma_R = -1$ then the switch state is ON, and if $\Gamma_R = 1$ the switch state is OFF. In order, to get the radiation pattern generated by each switch configuration, it is possible to get a complete antenna characterization by running the N_P full wave simulations, where for the ith simulation, a source to excite the ith port is used and other ports are terminated with a convenient load. Storing the vector of the currents I_{ip} computed in all ports and the far-fields $\vec{E}_{ip}(\theta, \phi)$ for each of the N_P simulations, the radiation pattern for arbitrary loading can be then computed [56]. The arbitrary values of the switches are given by superposition as :

$$\vec{E}_T(\theta, \phi) = \sum_{i=1}^{N_P} I_{ip} \vec{E}_{ip}(\theta, \phi) \quad (4.6)$$

In order to get the best antenna response, the collected data from (4.5) and (4.6) are introduced into a genetic algorithm that evaluates an specific

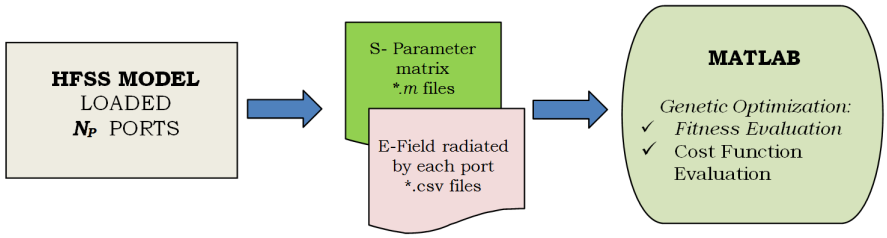

Figure 4.2 – General script Flow-chart of the Genetic optimization based on port load.

cost function to arrive at the optimal solution. In particular, the genetic algorithm stops when the antenna electrical specifications are obtained and the cost function is minimum. For the specific case of a reconfigurable RF repeater, there are some requirements that the repeater needs to fulfill: 1) Higher isolation between the Rx and TX ports $S^{RT}_{21,} \geq 60\,dB$, 2) good matching conditions in the Rx-TX ports $S^{Rx}_{11,}S^{Tx}_{22,} \leq -10\,dB$, and 3) the Rx maximum radiation pattern $\vec{E}^{Rx}_{max}$ pointing to a determined base station. For the mentioned electromagnetic antenna specifications the cost function has to minimize 1) and 2) and optimize 3). The cost function defined and used for the reconfigurable repeater is defined as

$$F_{cost} = w_1 \left(\frac{S^{RT}_{21,opt}(f_d) - S^{RT}_{21}(f_d)}{S^{RT}_{21,opt}(f_d)} \right)^2 + w_2 \left(\frac{S^{Rx}_{11,opt}(f_d) - S^{Rx}_{11}(f_d)}{S^{Rx}_{11,opt}(f_d)} \right)^2 + w_3 \left(\frac{S^{Tx}_{22,opt}(f_d) - S^{Tx}_{22}(f_d)}{S^{Tx}_{22,opt}(f_d)} \right)^2 + w_4 \vec{E}^{Rx}_{max}(f_d, \phi = 90^o, \theta^{Rx}_d) \quad (4.7)$$

where w_1, w_2, w_3, w_4 are the weighting functions , f_d is the desired operation frequency , θ^{Rx}_d is the desired DOA azimuth angle, $S^{RT}_{21,opt}$ is the desired isolation between Rx-Tx ports, $S^{Rx}_{11,opt}$ and $S^{Tx}_{22,opt}$ are the desired port return loss. The general genetic optimization flow chart script implemented with HFSS and matlab based on port loading is shown in Fig.4.2.

4.2 Isofrequency Reconfigurable 8 Bit RF Repeater

Based on the results of the Fig.3.12, with a total of 8 parasitic elements it is possible to have a good repeater performance in a realistic scatterer envi-

ronment. Using 8 parasitic elements, it was decided that, in order to reduce the repeater complexity, the maximum number of switching devices had to be the same. In order to minimize the number of switches, each switch has been placed in sensitive positions where the change on the currents along the parasitic elements produce important changes in the shape of the total radiated field. As mentioned before, the genetic algorithm is a powerful tool that helps to find the best repeater configuration, and is used to design the reconfigurable repeater presented in this part.

A realistic monopole-based isofrequency reconfigurable repeater is designed to operate at 5.25 GHz under the WIMAX frequency band, using a low number of switching devices. The proposed repeater has the capability to point its maximum of the radiation pattern towards a specific base station while maintaining good match and a high isolation level between the Rx and Tx ports. The repeater reconfiguration is achieved by changing the state of the PIN diodes, which are placed in selected positions on the parasitic elements. The repeater can be electronically reconfigured to react to changing scatterer environments, thus enhancing and recovering a similar isolation level to that obtained with an initial optimum configuration of parasitic strips in which no scatters were present.

The geometry of the proposed reconfigurable RF repeater is depicted in Fig.4.3. The repeater consists of two active monopoles separated by a vertical metallic plane. As started, the metallic plane is introduced to reduce the coupling between antennas. On each side of the metallic plane two groups of two reconfigurable parasitic dipole elements are symmetrically placed at a distance $d_{mp}^{Rx} = d_{mp}^{Tx}$ from the metallic plane behind each active dipole. The two pairs of parasitic monopoles of each group are separated by lateral distances s_{1p}^{Rx} and s_{2p}^{Rx} respectively. In order to maintain a compact size for the repeater, the size of the metallic plane was reduced to $\lambda/2 \times \lambda/2$.

As a first step towards finding the optimum position of these parasitic elements, the separation between them and the length of each parasitic element are calculated using a genetic algorithm with the goal of enhancing the isolation between the Tx and Rx ports in the absence of scatters. Secondly, the optimum distance d_{ma}^{Rx} of each active element to the metallic plane is found in this scenario. At that point, a study of sensitivity showed how the parasitic dipole position and length take an important role in maximizing the isolation level between ports for a given frequency, as well as in shaping the Rx or Tx radiation patterns of the repeater. This can be explained from the fact that depending on the length of the reconfigured parasitic strips, those can act as a reflector or director strip. Thus the change in the parasitic lengths produces a deviation in the angular direction of radiation that at the same time helps reducing the coupling between the Rx and Tx ports.

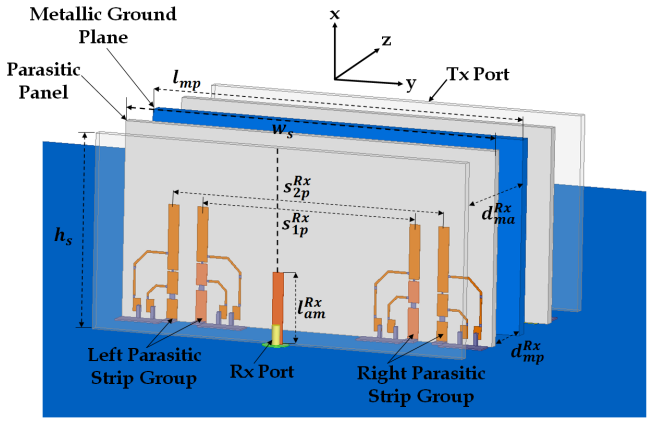

(a)

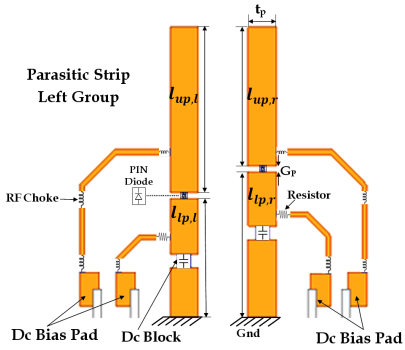

(b)

Figure 4.3 – (a) Isofrequency reconfigurable 8-bit RF repeater (b) Dimensions of the left parasitic strip group symmetrical to the right parasitic strip group.

A printed monopole version of the isofrequency reconfigurable repeater has been designed for its simplicity of fabrication and measurement, as shown in Fig.4.4. The repeater dimensions are optimized for the desired operating frequency at 5.25 GHz and to produce a maximum isolation level between the Rx and Tx ports while maintaining good impedance matching for different cases of scatters location. The optimum size of the repeater and the parasitic elements are shown in Table 4.1.

In order to optimize the repeater parasitic elements, the modeling PIN diode in "OFF" and "ON" state is an important parameter to be considered because the PIN diode present an impedance that can change the parasitic electric length. The PIN diode in "ON" and "OFF" state are modeled according to the equivalent circuit shown in Fig.4.5(a). The switch used in this work is a microwave GaAs PIN diode (model MA4AGBLP912, vendor

Repeater Optimum Dimensions (mm)		**Parasitic Strip Optimum Dimensions** (mm)	
$l_{am}^{Rx} = l_{am}^{Tx}$	**11**	$l_{lp,l}$	**7.5**
$d_{ma}^{Rx} = d_{ma}^{Tx}$	**22.52**	$l_{lp,r}$	**9.1**
$d_{mp}^{Rx} = d_{mp}^{Tx}$	**10**	$l_{up,l}$	**10**
w_s	**60**	$l_{up,r}$	**8.4**
h_s	**30**	t_p	**1.7**
$s_{1p}^{Rx} = s_{1p}^{Tx}$	**34.4**	G_p	**0.3**
$s_{2p}^{Rx} = s_{2p}^{Tx}$	**43.8**	w_{gnd}	**140**

Table 4.1 – Isofrequency reconfigurable 8-bit repeater optimum dimensions.

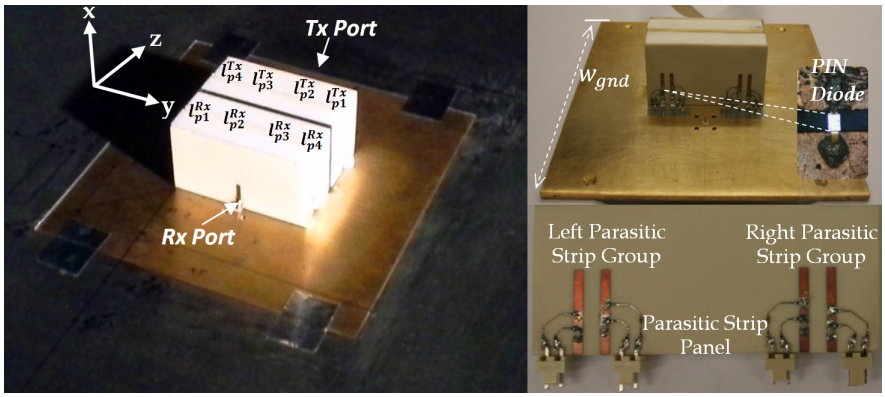

Figure 4.4 – Fabricated isofrequency repeater monopole version and zoom-in of the parasitic panel and bottom view. The PIN diodes are attached using silver epoxy.

MA-COM) with measured insertion loss 0.34 dB in "ON" mode fed with $10\,mA$ and 22 dB in "OFF" mode at 5.25 GHz (Fig.4.5 b).

The isofrequency repeater was designed using an electromagnetic full wave simulations tool (HFSS). To experimentally verify the design and to compare it with the simulated results, a prototype has been manufactured, where the active and parasitic elements are printed on a substrate RO4003 (ϵ_r =3.55, $tan\delta$ = 0.0027) with a thickness of 1.52 mm. The DC paths are designed to bias the PIN diodes and minimize any undesirable coupling with the parasitic strip elements. The parasitic monopole strips have been designed with an initial length of around $\lambda/2$ in such a way that when additional

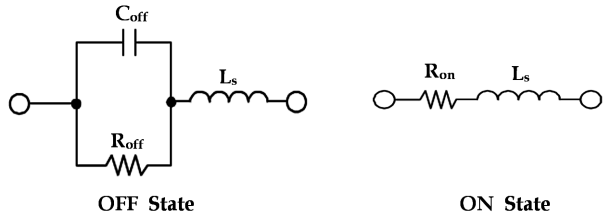

(a)

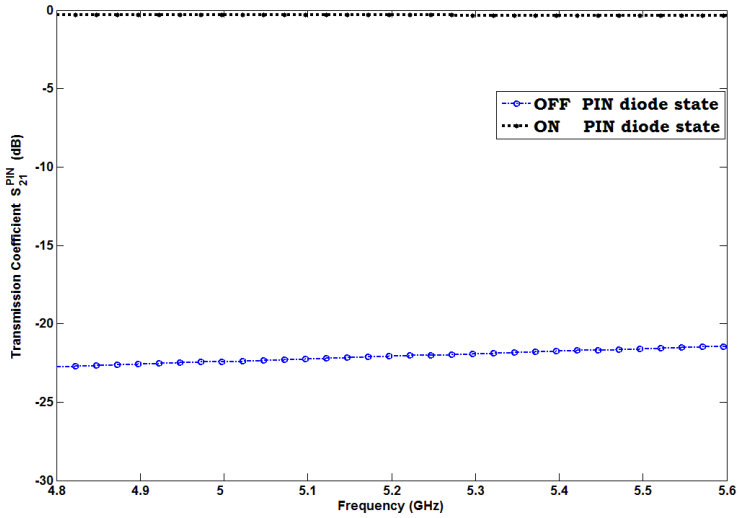

(b)

Figure 4.5 – (a) PIN diode model (b) Transmission coefficient S_{21}^{PIN} for the PIN diode values $C_{off} = 5.5\,fF$, $R_{off} = 8\,k\Omega$, $L_s = 0.3\,nH$, $R_{on} = 3.3\,\Omega$.

incremental strips connected by "ON" state switches are added they are slightly longer than λ/2 operating basically as reflectors elements. On the other hand when some strips are disconnected by "OFF" state switches the parasitic length is slightly shorter than λ/2 operating essentially as director elements. The "ON" state of the switches is referred with the symbolic notation value "1", and the "OFF" state with the symbolic value "0". Initially the Tx and the Rx parasitic strip panels are configured into a symmetrical state, which means that the radiation pattern in both ports has the same shape. The total number of different possible configurations with the current number of parasitic strip elements is 2^8. The radiation efficiency of the repeater antenna depends on the particular configuration of the ON-OFF PIN diodes distribution and varies between 85% and 90%.

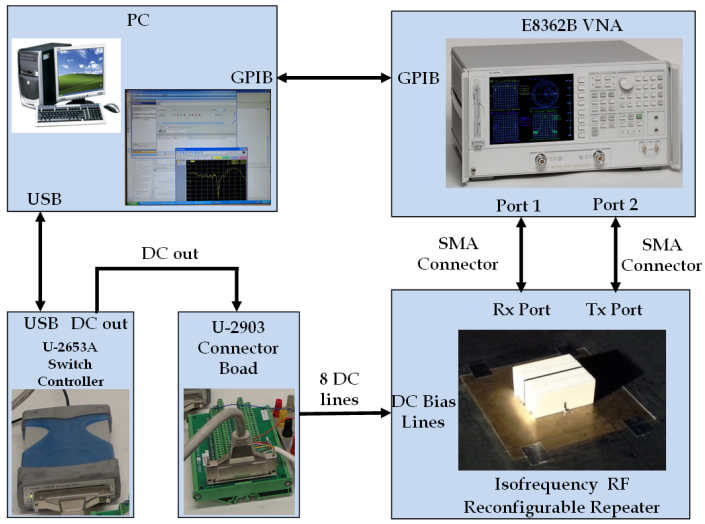

Figure 4.6 – Setup to characterize the reconfiguration properties of the 8-bit isofrequency repeater.

The repeater switch configuration state is applied using the commercial board (Agilent U-2653A) controlled by PC. The complete setup used to measure the repeater scattering parameters S is depicted in Fig.4.6. A similar measure setup has been used in the anechoic chamber in order to measure the repeater radiation pattern characteristics for different switch configurations with and without scatterer presence.

The optimization process has been performed using a genetic algorithm in combination with (HFSS), that consists on a custom-coded optimization algorithm running over matlab using a script to lunch the multiple required simulations. As a result, the optimum states of the switches in the parasitic elements were found using a genetic algorithm in combination with a multi-goal cost function (4.7) based on the isolation between ports, the impedance matching, and the shape of radiation patterns.

4.2.1 Isofrequency Reconfigurable 8-bit Repeater in absence of scatterers

In absence of scatterers, the measured initial isolation level between the Rx and the Tx ports without parasitic elements and separated only by the metallic plane in the absence of nearby obstacles is 36.5 dB at 5.25 GHz, this value is defined as the reference isolation level. In this case, when the parasitic strip elements are placed and configured to an optimum parasitic strip state, significant improvement into the matching level (up to -10 to -15 dB)

Configuration	DOA (Rx Port)	l_{p1}^{Rx}	l_{p2}^{Rx}	l_{p3}^{Rx}	l_{p4}^{Rx}	l_{p1}^{Tx}	l_{p2}^{Tx}	l_{p3}^{Tx}	l_{p4}^{Tx}
Conf. # 1	135^o	**1**	**0**	**0**	**0**	**1**	**0**	**0**	**0**
Conf. #2	150^o	**1**	**1**	**0**	**0**	**0**	**0**	**0**	**0**
Conf. #3	$\pm 180^o$	**0**	**0**	**0**	**0**	**0**	**0**	**1**	**1**
Conf. #4	-150^o	**0**	**0**	**1**	**1**	**0**	**0**	**0**	**0**
Conf. #5	-135^o	**0**	**0**	**0**	**1**	**0**	**0**	**1**	**0**

Table 4.2 – Optimum switch parasitic strip configuration in absence of scatterers

and isolation (up to 20 dB below initial levels) may be dynamically obtained for $1\% - 3\%$ frequency bandwidths. In the Rx port, the maximum radiation pattern is able to point to the DOA $= -135^o, -150^o, \pm 180^o, 150^o, 135^o$, which indicates that the repeater has radiation pattern flexibility and can get the maximum gain pointing to an specific base station. In the table 4.2 the bit configurations that fulfill the electromagnetic repeater specifications are presented . In the Fig.4.7 the simulated scattering S parameters for optimal configurations are presented, which are agree with the measured scattering S parameters presented in Fig.4.8. In the Fig.4.9 the comparison between the simulated and the measured radiation pattern for the repeater optimal configurations are presented , where can be seen that the simulated and measured values agree. In the repeater Rx port radiation pattern, for the configuration #3, in the direction of the maximum co-polar level, the measured cross-polar radiation is of 20dB below co-polar level when measured without the DC biasing networks. When measured with the bias networks, the value was 22 dB, thus a 2 dB increase was observed due to the biasing networks. This was considered acceptable for an indoor communication scenario. One of the repeater characteristics is that the Rx port is symmetric with the Tx port, and a wide radiation pattern in the Tx port is required to operate in an indoor place, consequently the repeater gain is not high. The repeater realized gain for the optimum configurations and the realized gain as a function of the frequency for the configuration # 3 that represents a direct path between the base station and the repeater is shown in Fig.4.10. From the presented results is observed that the repeater performance in free space is good and the simulation and the measurements are agree with the designed electromagnetic specifications.

In absence of scatterers, from the total 2^8configurations in which the repeater can be configured when no exist scatterers, the 5.48 % are optimal configurations that maximize the isolation to values around 60 dB, meaning

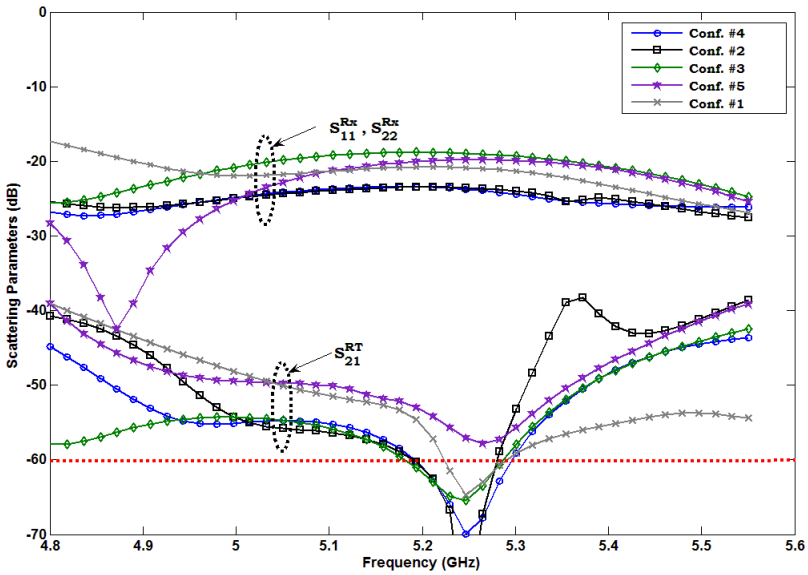

Figure 4.7 – Simulated scattering parameters of the 8-bit repeater optimum configurations in free space.

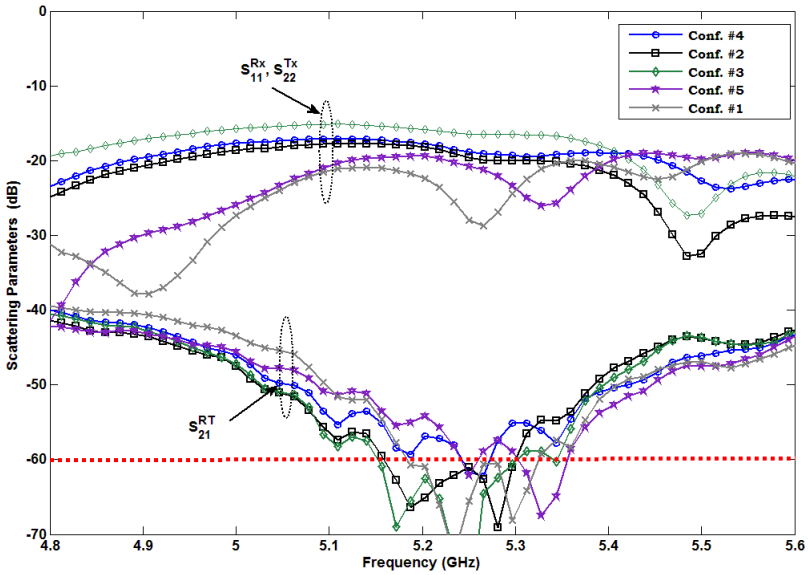

Figure 4.8 – Measured scattering parameters of the 8-bit repeater optimum configurations in free space.

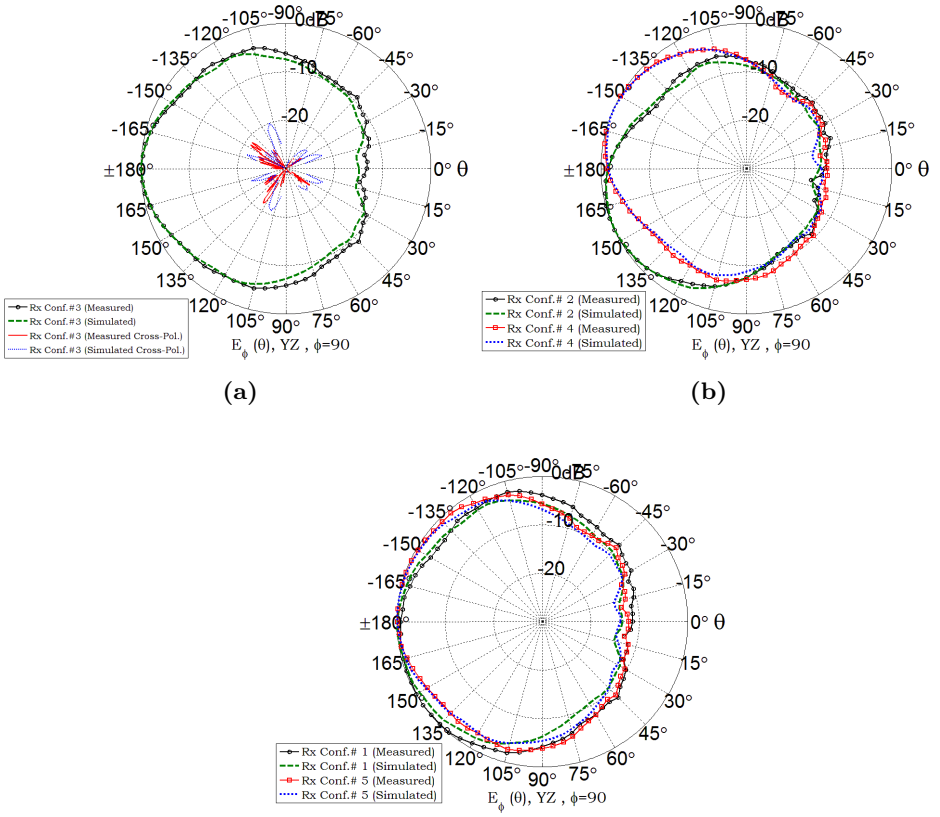

Figure 4.9 – Measured and simulated the repeater Rx port radiation pattern for the optimum configurations in free space. a) Conf. # 3 b) Conf. # 2 and Conf. # 4 c) Conf.# 1 and Conf.# 5.

that the repeater has more optimal configurations that enhance the isolation between the Rx-Tx ports (see Fig.4.11).

4.2.2 Isofrequency Reconfigurable 8-bit Repeater performance with the reference scatterers

In a real scatterer environment, the dimension and position of the scatterers is random and it change constantly, consequently the configuration and the position of the parasitic elements to compensate and recover a high isolation in the repeater Rx-Tx ports also has to change. A proposed way for designing a robust repeater able to work in a changing scatterer environment, is that starting from a repeater designed to operate in free space, define

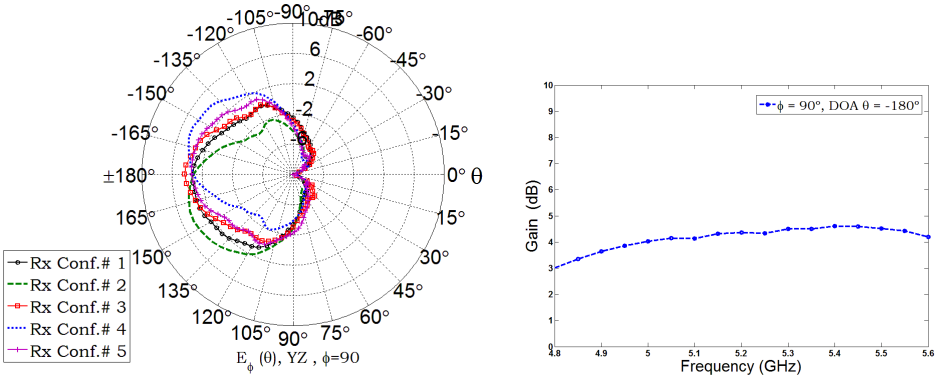

(a) **(b)**

Figure 4.10 – (a) Realized gain in the repeater Rx port for the optimal configurations (b) Repeater 8-bit gain for the optimal configuration #3 in the Rx port.

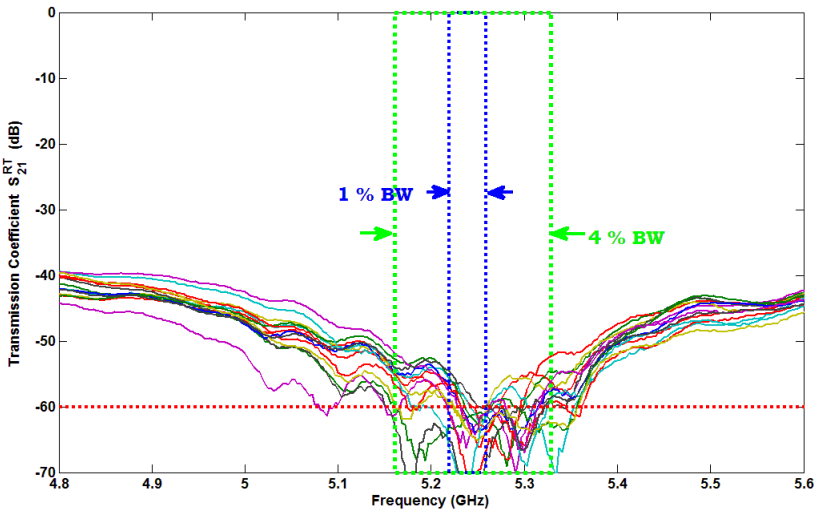

Figure 4.11 – Transmission coefficient $S_{21,}^{RTx}$ for all the possible optimal repeater configurations.

a set of reference scatterers that may be considered close to a worst real scenario. In this case, the scatterers have to be placed in a position where they generate the highest realistic maximum reflections possible, and, consequently if the repeater can be reconfigured under these conditions, then, the probability to properly operate in presence of realistic scatterers is increased. In order to attain this goal, three reference cases are considered : 1) a scatterer placed in a lateral position, 2) a scatterer rotated 45^o degrees and placed in lateral position, and 3) a plane $3\lambda \times 3\lambda$ scatterer placed in a frontal position.The proposed reconfigurable repeater has been designed to operate under a scattering environment. In order to verify the reconfiguration capability of the proposed repeater geometry, a study of the changes on the isolation level between ports due to nearby obstacles placed at different positions is performed.

For the first case 1), at the position $\vec{r}_{S1}^{Tx}\left(r_{S1}^{Tx}, \theta_{S1}^{Tx}, \phi_{S1}^{Tx}\right)$ is placed , a scatterer with dimensions of $0.53\lambda \times 0.53\lambda$ at $\vec{r}_{S1}^{Tx}\left(1.67\lambda, 76.35^o, 90^o\right)$, from the origin. When the lateral scatterer is introduced, the isolation level of 65 dB previously obtained at 5.25 GHz is reduced to 42 dB (using the parasitic strip optimum configuration when the repeater is in absence of scatterers). When the parasitic strip elements are re-optimized for the new scenario, the isolation level increases to 55 dB. Though the selected parasitic strip configuration tries to recover and maintain the initial proposed electrical requirements, a tradeoff exists between the achievable isolation on the active elements and the direction of maximum of the radiation pattern in the Rx port .The optimum configurations that tries to fulfill and maintain the initial electromagnetic repeater characteristics are presented in Table.4.3. The measured transmission coefficients S_{21}^{RT} for this case are shown in Fig.4.12 and in Fig.4.13 the measured reconfigured radiation pattern in the Rx and Tx ports are presented. For this case, from the total 2^8 configurations in which the repeater can be reconfigured, a 4.3% of optimum configurations as minimize the transmission coefficient S_{21}^{RT} covering a 3% of bandwidth, this can be seen in Fig.4.14.

As a second case, the previous scatterer is rotated 45^o in the plane YZ plane with respect to the Tx printed monopole panel and placed in the position $\vec{r}_{S1}^{Tx}\left(1.45\lambda, 36.48^o, 90^o\right)$. The isolation level at 5.25 GHz is reduced to 43 dB (when using the parasitic strip configuration for case 1), however, when the parasitic elements are reconfigured, the measured isolation level increases to 57 dB at 5.25 GHz. The optimum new reconfigured bit states for this case are presented in Table 4.4. The measured transmission coefficient S_{21}^{RT} using the bit configurations that fulfill the repeater electromagnetic characteristics are shown in Fig.4.15, and in Fig.4.16 are presented the corresponding measured radiation pattern in the Rx and Tx port. Also for the presented

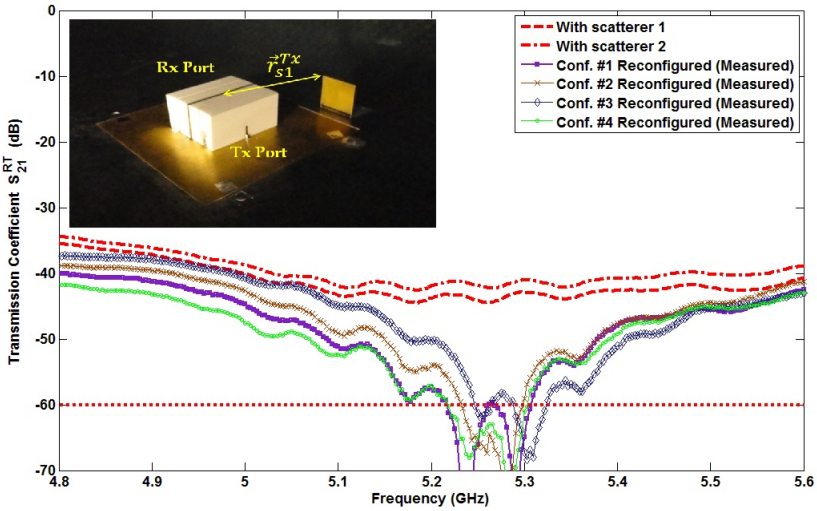

Figure 4.12 – Measured transmission scattering coefficients S_{21}^{RT} when is introduced a lateral scatterer.

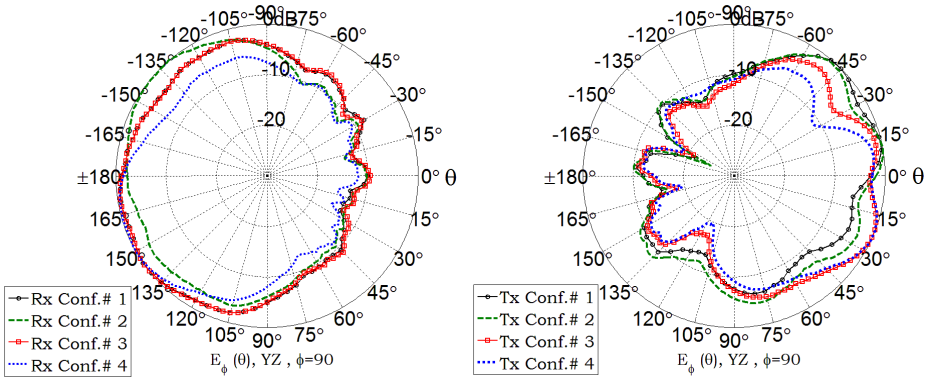

(a) **(b)**

Figure 4.13 – Measured reconfigured radiation pattern when of the isofrequency 8-bit repeater when a lateral scatterer is introduced. (a) Radiation pattern in the Rx port (b) Radiation pattern in the Tx Port.

Configuration	DOA (Rx Port)	l_{p1}^{Rx}	l_{p2}^{Rx}	l_{p3}^{Rx}	l_{p4}^{Rx}	l_{p1}^{Tx}	l_{p2}^{Tx}	l_{p3}^{Tx}	l_{p4}^{Tx}
Conf. # 1	135^o	**1**	**0**	**0**	**0**	**1**	**1**	**1**	**0**
Conf. #2	-135^o	**1**	**0**	**1**	**1**	**1**	**0**	**1**	**0**
Conf. #3	135^o	**1**	**0**	**1**	**0**	**1**	**0**	**1**	**1**
Conf. #4	150^o	**1**	**1**	**0**	**0**	**0**	**0**	**1**	**1**

Table 4.3 – Optimum switch parasitic strip configuration when is introduced a lateral scatterer.

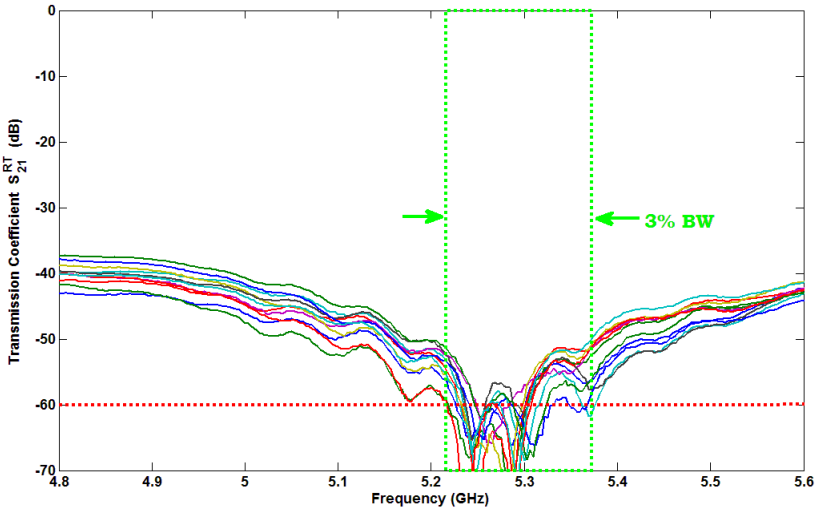

Figure 4.14 – Measured transmission coefficient $S_{21,}^{RT}$ for all the possible optimal repeater configurations when is introduced a lateral scatterer.

optimum configurations, from the total 2^8 configurations in which the repeater can be reconfigured, 6.64% of the total configurations minimize the transmission coefficient S_{21}^{RT} covering a 4.4% of bandwidth (See Fig.4.17) .

In these previous cases, the repeater reconfiguration capability has been evaluated in presence of nearby small scatterers, but the repeater also has to be designed to operate in presence of big scatterers producing significant reflections. A plane metallic scatterer placed in a frontal position can generate strong reflections over the field produced by the Tx repeater port, for this reason the repeater is tested to work in presence of this kind of scatterers. From the study realized in chapter 3, with eight parasitic elements, the repeater was capable to recover the high isolation when exist a metallic

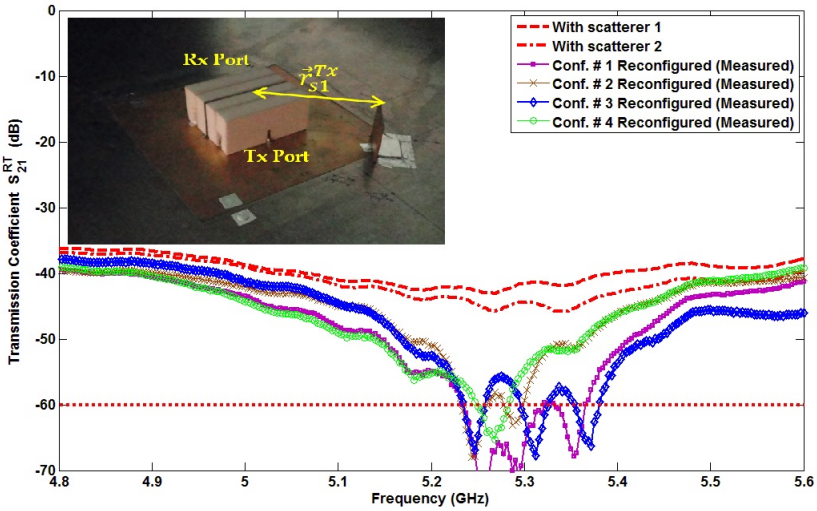

Figure 4.15 – Measured transmission scattering coefficients S_{21}^{RT} when is introduced a rotated 45^o scatterer.

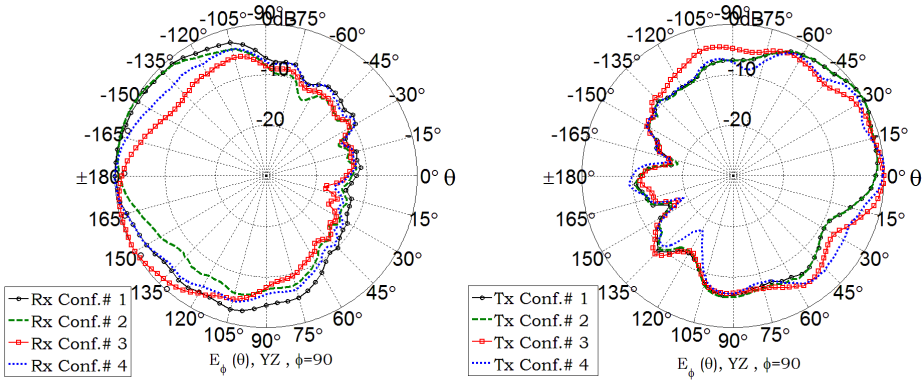

(a) **(b)**

Figure 4.16 – Measured reconfigured radiation pattern when of the isofrequency 8-bit repeater when a rotated 45^o scatterer is introduced. (a) Radiation pattern in the Rx port (b) Radiation pattern in the Tx Port.

Configuration	DOA (Rx Port)	l_{p1}^{Rx}	l_{p2}^{Rx}	l_{p3}^{Rx}	l_{p4}^{Rx}	l_{p1}^{Tx}	l_{p2}^{Tx}	l_{p3}^{Tx}	l_{p4}^{Tx}
Conf. # 1	-150^o	**0**	**0**	**0**	**1**	**1**	**1**	**1**	**0**
Conf. #2	-150^o	**0**	**1**	**1**	**1**	**1**	**1**	**1**	**0**
Conf. #3	150^o	**1**	**1**	**0**	**0**	**0**	**0**	**0**	**1**
Conf. #4	$\pm 180^o$	**0**	**0**	**0**	**0**	**1**	**1**	**1**	**1**

Table 4.4 – Optimum switch parasitic strip configuration when is introduced a rotated 45^o scatterer.

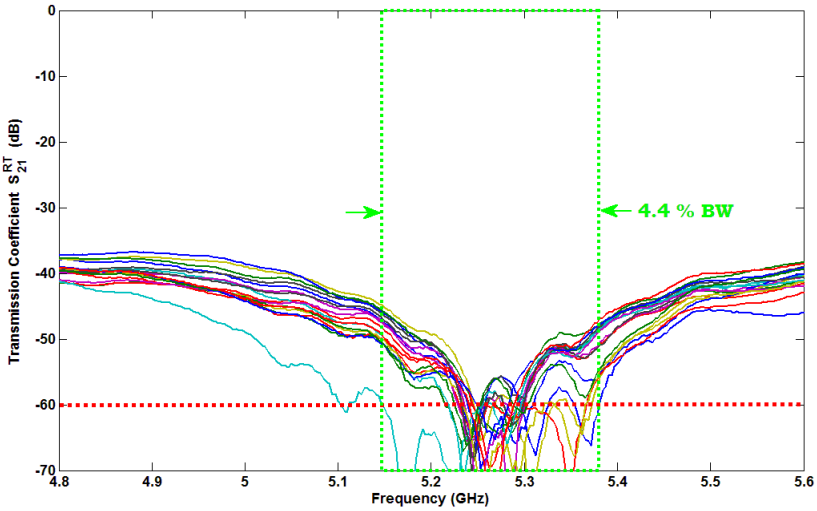

Figure 4.17 – Measured transmission coefficient $S_{21,}^{RT}$ for all the possible optimal repeater configurations when is introduced a rotated 45^o scatterer.

plane scatterer with dimension of $3\lambda \times 3\lambda$ at a minimum distance $r_{S1}^{Tx} = 9\lambda$ from the repeater Tx port. In order to design a repeater with high reconfigurable capabilities, the mentioned case is considered in the repeater design, but the metallic plane reflector is placed in a frontal position separated a distance $r_{S1}^{Tx} = 9\lambda$ from the repeater Tx port. The proposed prototype was measured in presence of the mentioned frontal scatterer, and the measured repeater transmission coefficient S_{21}^{RT} parameters for this case are presented in Fig.4.18. For this case the repeater is able to get a 6.2% of optimum bit states from the total 2^8 possible bit state configurations, covering a 1.06% isolation bandwidth of 60 dB.

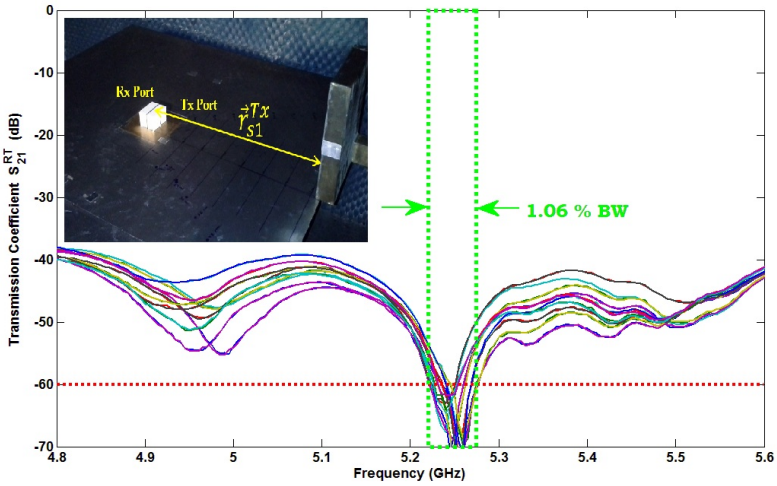

Figure 4.18 – Measured transmission coefficient $S_{21,}^{RT}$ for all the possible optimal repeater configurations when is introduced a plane $3\lambda \times 3\lambda$ frontal scatterer.

4.2.3 Isofrequency Reconfigurable 8-bit Repeater performance in a indoor scatterer environment

When the presented repeater prototype is capable to properly operate in presence of the reference scatterers, the next step is to evaluate the repeater in a real scatterer environment. Due the changing scatterer environment, is not possible to measure all the radiation patterns for each case, but it has been seen that the transmission coefficient S_{21}^{RT} parameter helps to evaluate the repeater performance which is easy and fast to measure for the used measurement setup. The repeater evaluation and measurement in an indoor location is realized taking in account three cases, 1) four scatterers placed in random position, 2) Evaluation of the repeater in a real indoor location (position 1) , and 3) evaluation of the repeater in a real indoor location (position 2) .

For the case 1, the closer scatterer is placed at a distance $r_{S1}^{Tx} = 8.4\lambda$ and the farthest scatterer is placed at a distance $r_{S2}^{Tx} = 12.76\lambda$. The measured transmission coefficients S_{21}^{RT} are presented in Fig.4.19, where it can be seen that the repeater is covering the 1.23% of the frequency bandwidth with high isolation, and from the total 2^8 possible configurations, the 5.07% are configurations with high isolation between Rx-Tx ports. In case 2, when the reconfigurable repeater is placed in a real indoor location, the bandwidth of high isolation $\geq 60dB$ covers a 1.04%, and, from the total possible 2^8 configurations, the 4.91% are optimal for the transmission coefficient S_{21}^{RT}

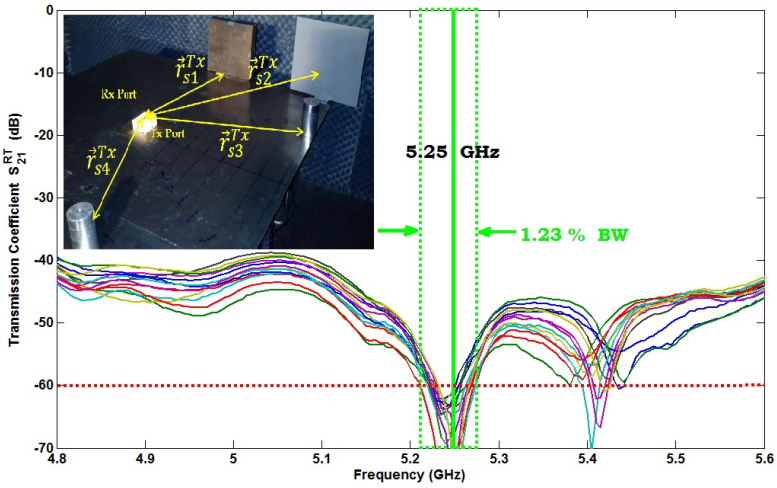

Figure 4.19 – Measured transmission coefficient $S^{RT}_{21,}$ for all the possible optimal repeater configurations in presence of four scatterers in random position (case 1).

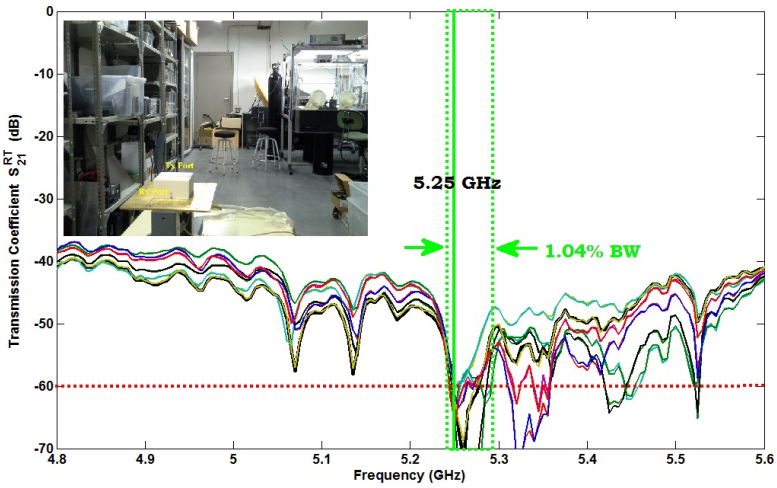

Figure 4.20 – Measured transmission coefficient $S^{RT}_{21,}$ for all the possible optimal repeater configurations in an indoor location (position 1).

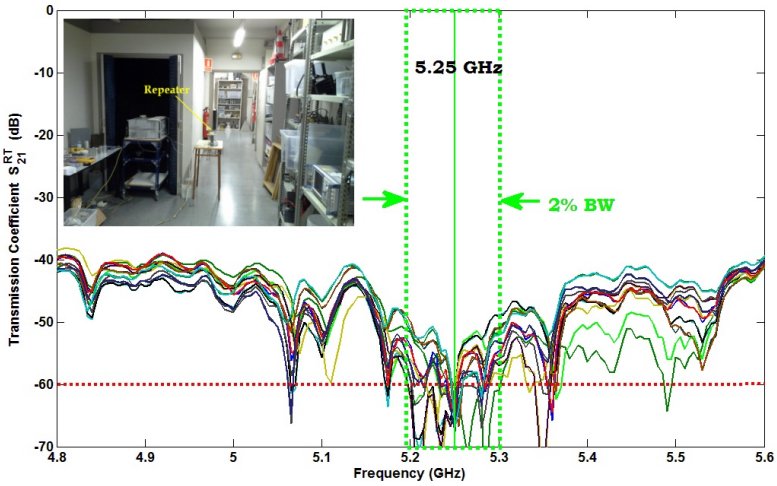

Figure 4.21 – Measured transmission coefficient $S_{21,}^{RT}$ for all the possible optimal repeater configurations in an indoor location (position 2).

(see Fig.4.20). Finally, for the case 3, the repeater presents a 2% bandwidth of high isolation covering the operation frequency of 5.25 GHz, where from all the possible 2^8 configurations, the 6.53% are optimal for the transmission coefficient S_{21}^{RT}, as it can be observed in Fig.4.21. With the presented results it has been demonstrated that the 8-bit reconfigurable repeater prototype presents high reconfigurable capability, low complexity and good performance in an indoor location with a realistic distribution of scatterers.

4.3 Frequency-Agile Isofrequency Repeater using a Reconfigurable Pixel Layer

In the previous sections it has been shown that a low complexity isofrequency reconfigurable repeater based on a modal study can work properly in a realistic scatterer environment. However the bandwidth of the presented isofrequency 8-bit reconfigurable repeater is narrow covering an effective high isolation bandwidth of 1% ∼2% in a real indoor location. In order to have a higher frequency bandwidth with high isolation reconfiguration capability, the complexity of the repeater had to be increased. An alternative isofrequency reconfigurable repeater prototype with high isolation frequency reconfiguration over a wide frequency range is presented in this section.

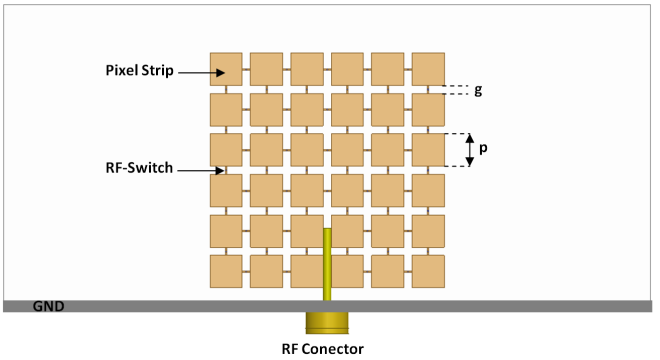

(a) Front view

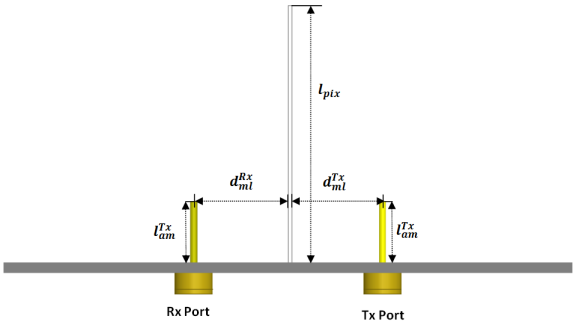

(b) Side view

Figure 4.22 – Pixel frequency-agile repeater geometry.

The repeater geometry is composed of two $\lambda/4$ monopoles with a common ground plane. The key and the most important part of the design consists on replacing the previous intermediate metallic plane by a reconfigurable plane. This reconfigurable layer is based on a pixeled geometry that consists in a grid of small metallic patches interconnected by RF-switches [57] [1]. The ON-OFF state configuration of the switches modifies the re-radiation of the pixel layer and therefore adjusts the repeater properties. The working principle is that the reconfiguration elements are not used to adjust the properties of either the Rx or Tx ports but, instead the reconfiguration elements affect simultaneously the two repeater ports in a balanced manner to adjust their mutual interaction. In Fig.4.22 the frequency-agile geometry is presented, where $g = 2mm$, $p = 12mm$, $l_{pix} = 120mm$, $d_{ml}^{Rx} = d_{ml}^{Tx} = 40mm$, $l_{am}^{Tx} = l_{am}^{Rx} = 27mm$.

[1] The manufactured pixeled layer used in the frequency-agile reconfigurable repeater has been provided by the collaboration with the Ph.D Daniel Rodrigo

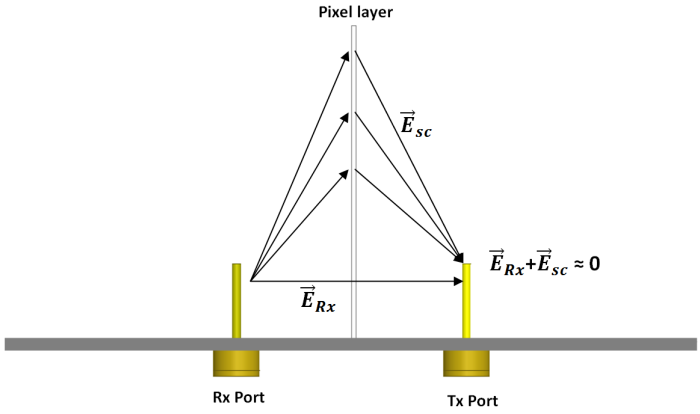

Figure 4.23 – Principle of operation of the pixel frequency-agile repeater.

The pixeled repeater operation principle is based on : the field produced at the Tx antenna location is the superposition of the field produced by the Rx antenna $\vec{E}_{Rx}$ and the field scattered by the pixel layer $\vec{E}_{sc}$. When the switch configuration on the pixeled layer is properly selected, the field scattered by the pixeled layer at the Tx antenna location cancels the direct radiation of the first antenna, providing in this way a high level of isolation, see Fig.4.23. Additionally, the repeater can be designed in such a way that the pixel layer induces a specific impedance loading over the Rx and Tx able to adjust their input impedances. Therefore, in principle it is possible to select configurations over a wide frequency range that produce simultaneously a low return loss and high isolation.

4.3.1 Frequency-Agile repeater design and optimization

The pixel frequency agile repeater has been designed to operate at 2.5GHz, and the pixel layer has been designed according to the guidelines given in [57], using a 6×6 pixel layer with individual pixel sized of $\lambda/10 \times \lambda/10$. The parameters $l_{am}^{Tx} = l_{am}^{Rx}$ and $d_{ml}^{Rx} = d_{ml}^{Tx}$ shown in Fig.4.22 b have been optimized to maximize the frequency reconfiguration range. In order to perform the optimization using an accurate and time-efficient process, the port loading technique has been used. For the proposed repeater it has been possible to compute the response of several thousands of switch configurations in a few minutes. The pixel frequency-agile repeater shown in Fig.4.24 has been manufactured in order to realize the frequency isolation reconfiguration flexibility.

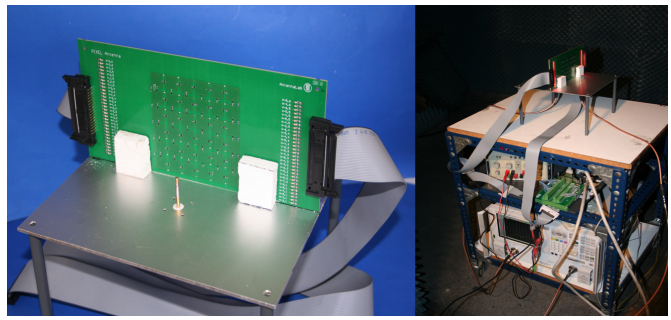

Figure 4.24 – Manufactured pixel frequency-agile repeater using a switched pixel layer with PIN diodes operating as RF-switches.

The resulting simulated and measured transmission coefficients S_{21}^{RT} provided by the optimized pixeled repeater are shown in Fig.4.25 and Fig.4.26. Each curve represents the optimum value of isolation at each central frequency. The optimal configuration at the frequency f_o is defined as the configuration with higher isolation at f_o among all the configuration with a reflection coefficient below -10dB at that same frequency. Therefore, high isolation and good matching are simultaneously achieved. The frequency agile reconfiguration range covers from 2.15 GHz up to 3.25 GHz, which means a reconfiguration bandwidth higher than 40 %. The isolation levels of the optimal configurations are between 60 dB and 70dB. This is 30 dB higher than the isolation achieved by an identical repeater replacing the pixel layer by a metallic plane reflector with same dimensions.

On the other hand, Fig.4.25 and Fig.4.26 also reflects that the instantaneous bandwidth of the optimal configurations is approximately 20 MHz. However this value can be improved by updating the fitness criteria to get a wider bandwidth. The optimal configuration is then redefined as the one that maximizes the worst case and consequently a wider bandwidth is obtained, based on this principle a bandwidth isolation of 60 MHz has been obtained. In Fig.4.27 and Fig.4.28 the simulated and measured transmission coefficients S_{21}^{RT} are presented for a bandwidth of 60MHz with a good agreement. With this study is clear that configurations covering a wider band can also be synthesized at the price of a lower isolation level. The frequency agile repeater gain is similar to the 8-bit reconfigurable repeater presented in the last section, it can be observed in Fig.4.29 where for the frequency 2.4 GHz the maximum realized gain is 4.89dB and for 2.5 GHz the realized gain is 4.80dB.

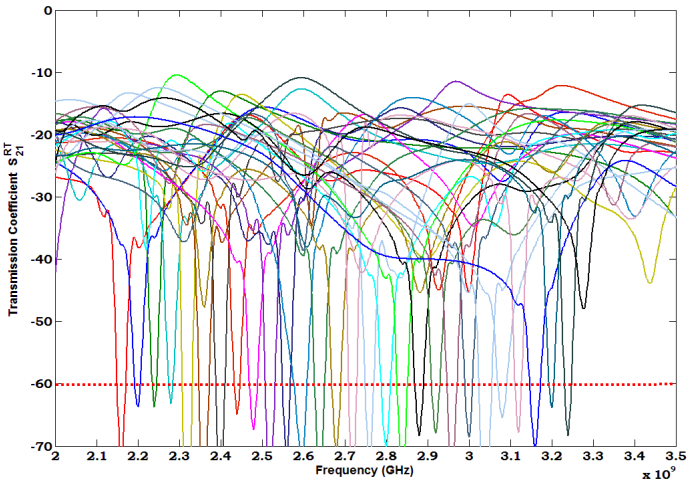

Figure 4.25 – Simulated transmission coefficient S_{21}^{RT} achieved by the optimal configurations of the pixel repeater for instantaneous bandwidth of 20 MHz at different frequency.

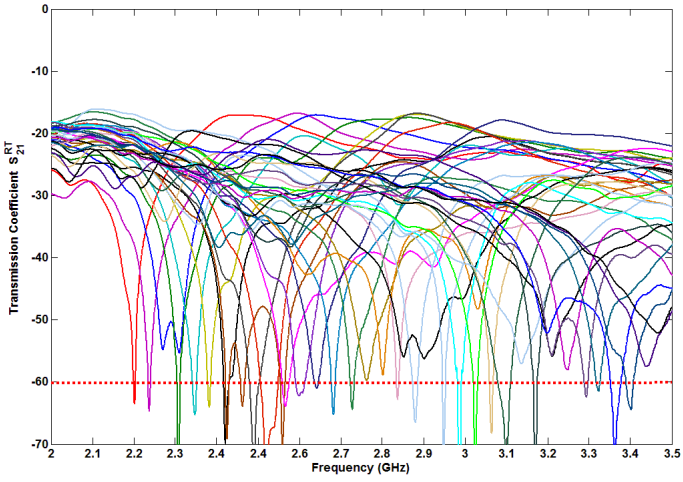

Figure 4.26 – Measured transmission coefficient S_{21}^{RT} achieved by the optimal configurations of the pixel repeater for instantaneous bandwidth of 20 MHz at different frequency.

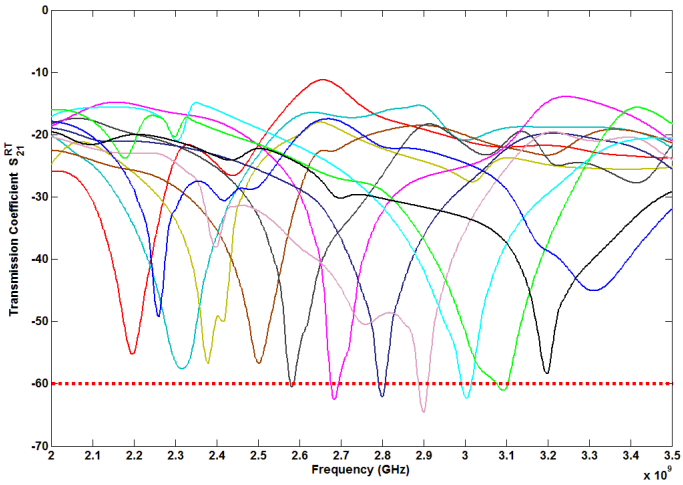

Figure 4.27 – Simulated transmission coefficient S_{21}^{RT} achieved by the optimal configurations of the pixel repeater for instantaneous bandwidth of 60 MHz at different frequency.

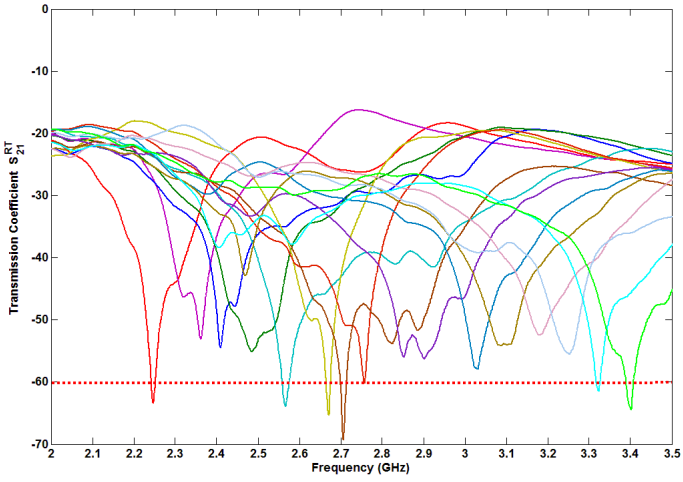

Figure 4.28 – Measured transmission coefficient S_{21}^{RT} achieved by the optimal configurations of the pixel repeater for instantaneous bandwidth of 60 MHz at different frequency.

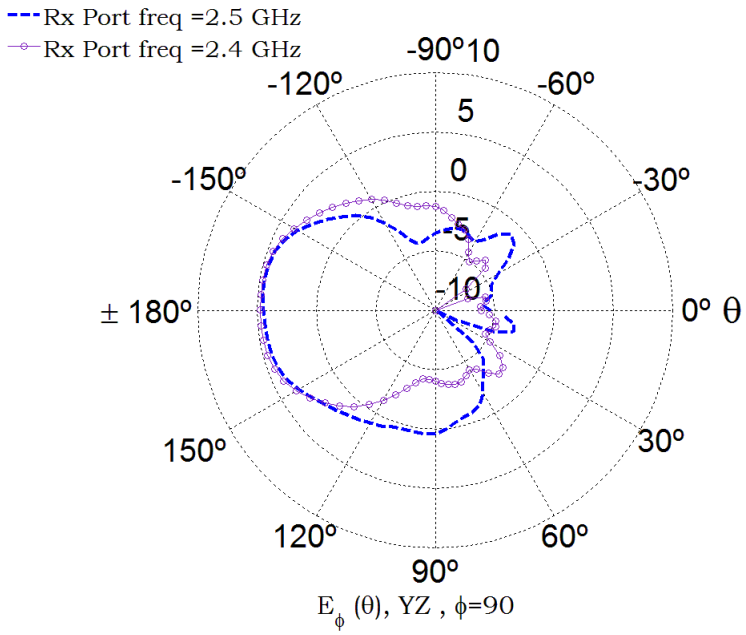

Figure 4.29 – Simulated frequency agile repeater gain for the instantaneous bandwidth of 60 MHz at the frequency of 2.4GHz and 2.5GHz .

Chapter 5

Conclusions And Discussion

This thesis has mainly contributed to the analysis, modeling and design of isofrequency reconfigurable repeaters able to operate in a proper way into realistic indoor locations maintaining good electromagnetic characteristics. This final chapter is devoted to present the main conclusions of this work. The main future research lines are also outlined.

5.1 Main Conclusions

The reconfigurable antennas is a promising solution for the communication systems when looking to improve the channel capacity and/or to extend the signal coverage. The main advantage of the reconfigurable antennas are the capabilities to change their frequency, polarization and radiation beam steering at a low cost. Reconfigurable antenna capabilities requires to operate in a determined changing environment keeping good electromagnetic characteristics. The design of reconfigurable RF repeaters is a relevant application of this reconfigurable antenna principle. In this thesis it has been shown that the use of a set of reconfigurable parasitic elements as part of the repeater, gives the flexibility to adapt the repeater electromagnetic characteristics to changing environments while keeping a good system performance. It has been proven with a low number of reconfigurable parasitic elements that allows to keep a low level of complexity it is possible to significantly reduce the coupling between Rx and Tx ports in a realistic scattering dynamic environment. The main difficult for the design of this kind of repeaters resides on the determination of the minimum number of parasitic elements. A modal study has been proposed to define the minimum number of parasitic elements able to obtain the specified Rx antenna pointing direction, impedance matching and isolation. As a significant contributions we may identify the following.

Modal Study Based on Spherical Wave Expansion

The spherical wave expansion theory can be used as an analytical tool for computing the mutual coupling between the Rx and Tx repeater antennas at different distances. Taking the advantage that the electromagnetic field can be decomposed in a series of spherical coefficients, a modal study for reducing the coupling between the two antennas has been realized. It has been observed that when the parasitic elements are used as part of the repeater, depending of their electrical length and position, they change the amplitude and phase of the spherical coefficients in a way that allows to extract some basic rules to establish a minimum number of parasitic elements into the repeater Rx-Tx system. As a first step, a repeater with one and two scatterers around it has been modeled, and the total repeater electromagnetic field has been decomposed in their spherical coefficients in order to identify the incremental coefficients generated by the scatterers. Different configurations of the parasitic elements and their influence over a determined area of the spherical coefficients modal (m, n) map has been studied. The modal map variation produced by the nearby scatterers is useful to guide the process of defining the number, dimensions and location of the parasitic dipoles to compensate the effect introduced by a certain

number of scatterers, located at different distances. Although this results are for a specific case, they can be used as a reference for general cases, because the scatterers are located where the reflections that they produce over the repeater are strongest (worst case). From this results has been found that for a realistic scenarios with an approximate number of eight parasitic elements the repeater has good reconfigurable capabilities.

Reconfigurable Repeater Prototype

In order to validate the previous analytical results, different reconfigurable repeater prototypes have been manufactured. The first manufactured repeater prototype uses four pixeled parasitic elements able to change their length in incremental steps. In order to reduce the repeater complexity, the pixeled parasitic elements has been placed in sensitive positions where the changes in their length produces significant changes on the isolation between the Rx and Tx antenna. The optimization of the repeater has been done with the help of a genetic algorithm in order to find the optimum repeater configuration and it has been obtained 60 dB of isolation between the Rx and the Tx antenna at the designed frequency. In order to explore the reconfigurable capabilities it has been considered two reference cases in which a scatterer is placed at two different positions around the repeater system. In both cases the length of the parasitic elements were reconfigured and it has been observed that a similar isolation level obtained initially with the parasitic elements without any scatterer around the repeater at the operation frequency can be approximately recovered. Although the obtained bandwidth of the maximum isolation is narrow, this results are important because they give an important base for designing reconfigurable repeaters based on a set of parasitic reconfigurable elements.

The second manufactured repeater prototype uses eight reconfigurable parasitic elements and is the first reconfigurable repeater based on a small number of switches electronically controlled reported on publications. This prototype not only has the capability to enhance and recover the isolation level at the designed operation frequency, but also has the flexibility to aim the Rx radiation pattern to a determined direction in the azimuth plane. The presented prototype has good electromagnetic characteristics, and has been measured for different scatterer environments. The measured results have shown that the repeater has a good performance with high reconfigurable capabilities for realistic indoor locations.

Finally a third manufactured repeater based on a pixeled layer as reconfigurable mechanism has been designed and measured. The reconfigurable capabilities of this prototype has been studied obtaining high reconfigurable frequency isolation capabilities over a wide frequency range. This

novel structure has contributed to determine the frequency isolation reconfigurable limits of this kind of repeaters.

5.2 Future Work

Future research lines move towards the real implementation of the 8-bit reconfigurable repeaters for indoor locations. The presented work paves the way for developing reconfigurable repeaters for operating in different scatterer environments while maintaining good electromagnetic characteristics.

In the case of the frequency-agile repeater using a reconfigurable pixeled layer, it uses a high number of switching elements. For this design, a study in how to reduce the number of switches and the system complexity is still an open research topic line that requires additional work.

Finally, the repeater optimization algorithms is an open research line that needs to be explored for developing new reconfigurable smart RF devices using reconfigurable antennas.

List of Figures

List of Tables

List of Symbols

η	Intrinsic impedance in vacuum
λ	Wave length
θ_{Si}	Angle of the direction of a determined Si scatterer
$\vec{E}^{Rx}$	Electric field generated by the Rx antenna
$\vec{E}^{Tx}$	Electric field generated by the Tx antenna
$\vec{E}^{Rx}_{ad}$	Electric field generated by the Rx active dipole
$\vec{E}^{Tx}_{ad}$	Electric field generated by the Tx dipole
$\vec{E}_{ip}$	Far field given by the ith port radiation pattern
$\vec{E}^{Rx}_{p1}$	Electric field generated by the Rx parasitic 1 in the right side
$\vec{E}^{Tx}_{p1}$	Electric field generated by the Tx parasitic 1 in the right side
$\vec{E}^{Rx}_{p2}$	Electric field generated by the Rx parasitic 2 in the left side
$\vec{E}^{Tx}_{p2}$	Electric field generated by the Tx parasitic 2 in the left side
$\vec{E}^{Tx}_{Si}$	Scattered electric field generated by a determined Si scatterer number
$\vec{E}^{Rx}_{sm}$	Scattered Electric field generated by the metallic plane over the Rx side.

$\vec{E}_{sm}^{Tx}$ Scattered Electric field generated by the metallic plane over the Tx side.

$\vec{E}_T$ Far field given by arbitrary switch configuration on reconfigurable antennas

$\vec{r}_p$ Vector of relative position between the Rx and Tx antenna

$\vec{r}_{so}^{rx}$ Position of the plane surface with respect to the Rx antenna

$B_n^{(rep,par)}$ Repeater spherical wave coefficients. This coefficients are refered when the Rx-Tx Ports are separated by a metallic plane reflector and using a determined number of parasitic elements.

B_n^{rep} Reference spherical wave coefficients. This coefficients are refered when the Rx-Tx Ports are separated only by a metallic plane reflector.

d_{ds}^{rt} distance separation between the Rx and the Tx active dipole

d_{ma}^{Rx} Distance from the metallic plane reflector to the Rx active dipole

d_{ma}^{Tx} Distance from the metallic plane reflector to the Tx active dipole

d_{ml}^{Rx} distance from the Rx monopole to the pixel layer

d_{ml}^{Tx} distance from the Tx monopole to the pixel layer

d_{mp}^{Rx} Distance from the metallic plane reflector to the parasitic elements in the Rx antenna

d_{mp}^{Tx} Distance from the metallic plane reflector to the parasitic elements in the Tx antenna

d_{sa}^{rx} Distance from the plane surface So to the Rx dipole

d_{sa}^{tx} Distance from the plane surface So to the Tx dipole

F_{cost} Is the cost function used in the genetic algorithm to research the isofrequency reconfigurable repeater optimum electric specifications.

g Separation between pixel strips

$h_n^{(1)}$ Spherical hankel function of first kind

h_s Height of the parasitic reconfigurable panel

I_a Current through the active element

I_{ip}	Current applied to the ith port network
I_p	Current through the parasitic element
I_{Rx}	Input current in the Rx antenna
I_{Tx}	Input current in the Tx antenna
k	Wave number in vacuum $2\pi/\lambda$
l_{ad}^{Rx}	Length of the active dipole Rx
l_{ad}^{Tx}	Length of the active dipole Tx
l_{ef}^{Rx}	Efective lenght of the Rx dipole
l_{ef}^{Tx}	Efective lenght of the Tx dipole
l_{lp}	Length of the lower parasitic element
l_{mp}	Length of the metallic plane
l_{p1}^{Rx}	Length of the right parasitic one in the Rx antenna
l_{p1}^{Tx}	Length of the right parasitic one in the Tx antenna
l_{p2}^{Rx}	Length of the left parasitic two in the Rx antenna
l_{p2}^{Tx}	Length of the left parasitic two in the Tx antenna
l_{pix}	Length of the pixel layer
l_p	Total parasitic length when all the parasitic elements are considered equal
l_{up}	Length of the upper parasitic element
p	Pixel strip size
P_n^m	Associated legendre polynomials
r_{Si}^{Tx}	Minimum distance from the repeater to the closer scatterer in the Tx side.
r_{sp}^{Rx}	Radii of the sphere that surrounds the Rx antenna
r_{sp}^{Tx}	Radii of the sphere that surrounds the Tx antenna
S_{1p}^{Rx}	Lateral separation between the parasitic one and the parasitic two in the Rx antenna

S_{1p}^{Tx}	Lateral separation between the parasitic one and the parasitic two in the Tx antenna
S_{21}^{PIN}	Transmition coefficient of the PIN diode in ON or OFF state
t_p	Width of the metallic pixel strip
V_{Rx}	Receiving coupled voltaje in Rx antenna due the presence of the Tx antenna.
W_s	Width of the parasitic reconfigurable panel
Z_{11}^{ad}	Active dipole self impedance
Z_{11}^{Rx}	Rx antenna self-impedance
Z_{12}^{RT}	Mutual coupling impedance between Rx-Tx antenna
Z_{21}^{pd}	Mutual impedance of the active dipole and the parasitic dipole
Z_{22}^{pd}	Parasitic dipole self impedance
Z_{22}^{Tx}	Tx antenna self-impedance
Z_{in}^{ad}	Input impedance of the active dipole

List of Publications

JOURNAL ARTICLES

- Rodrigo, D. ; **Diaz, E.** ; Jofre, L. " ***Reconfigurable Pixel-Layer Isolator For Frequency Tunable On-Frequency Repeaters***". , IEEE Antennas and Wireless Propagation Letters . (Summited 19-Sep-2013)

- ***Diaz, E.*** ; Grau, A. ; De Luis, J.R. ; De Flaviis, F. ; Jofre, L. *"**Isofrequency-Reconfigurable 8-Bit RF Repeater**"* . Antennas and Wireless Propagation Letters, IEEE Volume: 10, Publication Year: 2011 , Page(s): 1239 - 1242 .

CONFERENCE ARTICLES

- ***Diaz, E.***; De Luis, J.R. ; Grau, A. ; De Flaviis, F. ; Jofre, L. *"**Pixeled-dipole based isofrequency reconfigurable RF repeater**"*. Antennas and Propagation (EUCAP), Proceedings of the 5th European Conference on Publication Year: 2011 , Page(s): 2298 - 2301.

- D. Rodrigo, ***E. Diaz***, J. Romeu, and L. Jofre, *"**Frequency-agile on-channel repeater using a reconfigurable pixel layer**"*, in Proc. Seventh European Conf. Antennas and Propagation (EUCAP), Year: 2013.

Bibliography

[1] Y. Huang, N. Yi, and X. Zhu, "Investigation of using passive repeaters for indoor radio coverage improvement," in *Antennas and Propagation Society International Symposium, 2004. IEEE*, vol. 2, 2004, pp. 1623–1626 Vol.2.

[2] Y. Serizawa, Y. Watanabe, and S. Takeshita, "Multipath propagation effects on digital radio equipped with a plane reflector repeater," *Communications, Speech and Vision, IEE Proceedings I*, vol. 139, no. 2, pp. 176–180, 1992.

[3] H. Hristov, R. Feick, and W. Grote, "Improving indoor signal coverage by use of through-wall passive repeaters," in *Antennas and Propagation Society International Symposium, 2001. IEEE*, vol. 2, 2001, pp. 158–161 vol.2.

[4] C. Colavito and G. D'Auria, "Experimental research on the behavior of passive repeaters," *Proceedings of the IEEE*, vol. 51, no. 11, pp. 1423–1430, 1963.

[5] Y. Lee, J. Kim, J. Ha, J. Choi, S. U. Seo, Y. Lee, and W. Seong, "Design of a microstrip patch array antenna for wcdma indoor repeater systems," in *Electromagnetics in Advanced Applications, 2009. ICEAA '09. International Conference on*, 2009, pp. 361–364.

[6] P. J. Stevens, "Repeaters in pcn and mobile cellular networks," in *Radio Receivers and Associated Systems, 1995., Sixth International Conference on*, 1995, pp. 154–157.

[7] K.-S. Min, D.-J. Kim, and Y.-M. Moon, "Improved mimo antenna by mutual coupling suppression between elements," in *Wireless Technology, 2005. The European Conference on*, 2005, pp. 125–128.

[8] H. Wang, D. Fang, and X. L. Wang, "Mutual coupling reduction between two microstrip patch antennas by using the parasitic elements," in *Microwave Conference, 2008. APMC 2008. Asia-Pacific*, 2008, pp. 1–4.

[9] A. S. M. Marzuki, A. R. A. Rahim, B. Mohmd, K. Khalil, A. Naemat, and A. Tee, "Antenna isolation considerations in wcdma repeater deployment," in *RF and Microwave Conference, 2006. RFM 2006. International*, 2006, pp. 347–350.

[10] N. Michishita, H. Arai, and Y. Ebine, "Mutual coupling characteristics of patch array antenna with choke for repeater systems," in *Antennas and Propagation, 2003. (ICAP 2003). Twelfth International Conference on (Conf. Publ. No. 491)*, vol. 1, 2003, pp. 229–232 vol.1.

[11] W. Kim, M. Yoo, S. Park, H. Ko, H. Lee, J. Shin, Y.-S. Chung, and C. Cheon, "Design of a single body type repeater antenna for isolation enhancement at imt-2000 band," in *Antennas and Propagation Society International Symposium, 2009. APSURSI '09. IEEE*, 2009, pp. 1–4.

[12] W. T. Slingsby and J. McGeehan, "Antenna isolation measurements for on-frequency radio repeaters," in *Antennas and Propagation, 1995., Ninth International Conference on (Conf. Publ. No. 407)*, 1995, pp. 239–243 vol.1.

[13] J. Rahola and J. Ollikainen, "Analysis of isolation of two-port antenna systems using simultaneousmatching," in *Antennas and Propagation, 2007. EuCAP 2007. The Second European Conference on*, 2007, pp. 1–5.

[14] Y. Rikuta, H. Arai, and Y. Ebine, "Mutual coupling suppression of two dipole antennas backed by optimized reflector," in *Antennas and Propagation Society International Symposium, 2002. IEEE*, vol. 2, 2002, pp. 276–279 vol.2.

[15] ——, "Reflector shape optimization for fb ratio of dipole antenna," in *Microwave Conference, 2001. APMC 2001. 2001 Asia-Pacific*, vol. 3, 2001, pp. 1068–1071 vol.3.

[16] ——, "Enhancement of fb ratio for cellular base station antenna by optimizing reflector shape," in *Antennas and Propagation Society International Symposium, 2001. IEEE*, vol. 3, 2001, pp. 456–459 vol.3.

[17] S. Kim, J. Lee, J. Lee, J. Kim, B. Lee, and N. Kim, "Adaptive feedback interference cancellation system (af-ics)," in *Microwave Symposium Digest, 2003 IEEE MTT-S International*, vol. 1, 2003, pp. 627–630 vol.1.

[18] M. Lee, B. Keum, Y. Son, J.-W. Kim, and H.-S. Lee, "A new low-complex interference cancellation scheme for wcdma indoor repeaters," in *Computational Technologies in Electrical and Electronics Engineering, 2008. SIBIRCON 2008. IEEE Region 8 International Conference on*, 2008, pp. 457–462.

[19] P. Slobodzian, "Estimation of the repeater gain required for a wireless link," in *Microwaves, Radar and Wireless Communications, 2004. MIKON-2004. 15th International Conference on*, vol. 2, 2004, pp. 656–659 Vol.2.

[20] T. Jennifer, *Reconfigurable Antennas*, M. . C. publishers, Ed. Synthesis lectures on antennas num. 4, University of Illinois at Urbana-Champaign,Edit, 2007.

[21] L. Pringle, P. Harms, S. Blalock, G. Kiesel, E. Kuster, P. Friederich, R. Prado, J. Morris, and G. Smith, "A reconfigurable aperture antenna based on switched links between electrically small metallic patches," *Antennas and Propagation, IEEE Transactions on*, vol. 52, no. 6, pp. 1434–1445, 2004.

[22] B. Cetiner, H. Jafarkhani, J.-Y. Qian, H. J. Yoo, A. Grau, and F. De Flaviis, "Multifunctional reconfigurable mems integrated antennas for adaptive mimo systems," *Communications Magazine, IEEE*, vol. 42, no. 12, pp. 62–70, 2004.

[23] J. Maloney, M. Kesler, L. Lust, L. Pringle, T. Fountain, P. Harms, and G. Smith, "Switched fragmented aperture antennas," in *Antennas and Propagation Society International Symposium, 2000. IEEE*, vol. 1, 2000, pp. 310–313 vol.1.

[24] L. Pringle, P. Friederich, S. Blalock, G. Kiesel, P. Harms, D. Denison, E. Kuster, T. Fountain, and G. Smith, "Gtri reconfigurable aperture design," in *Antennas and Propagation Society International Symposium, 2002. IEEE*, vol. 1, 2002, pp. 473–476 vol.1.

[25] Z. Yao, S. Chen, S. Eshelman, D. Denniston, and C. Goldsmith, "Micromachined low-loss microwave switches," *Microelectromechanical Systems, Journal of*, vol. 8, no. 2, pp. 129–134, 1999.

[26] H.-P. Chang, J. Qian, B. Cetiner, F. De Flaviis, M. Bachman, and G. P. Li, "Rf mems switches fabricated on microwave-laminate printed circuit boards," *Electron Device Letters, IEEE*, vol. 24, no. 4, pp. 227–229, 2003.

[27] ——, "Design and process considerations for fabricating rf mems switches on printed circuit boards," *Microelectromechanical Systems, Journal of*, vol. 14, no. 6, pp. 1311–1322, 2005.

[28] A. Grau, J. Romeu, L. Jofre, and F. de Flaviis, "A software defined mems-reconfigurable pixel-antenna for narrowband mimo systems," in *Adaptive Hardware and Systems, 2008. AHS '08. NASA/ESA Conference on*, 2008, pp. 141–146.

[29] B. Cetiner, L. Jofre, J. Qian, S. Liu, G. P. Li, and F. De Flaviis, "A compact broadband mems-integrated diversity system," *Vehicular Technology, IEEE Transactions on*, vol. 56, no. 2, pp. 436–444, 2007.

[30] A. Grau, M.-J. Lee, J. Romeu, H. Jafarkhani, L. Jofre, and F. De Flaviis, "A multifunctional mems-reconfigurable pixel antenna for narrowband mimo communications," in *Antennas and Propagation Society International Symposium, 2007 IEEE*, 2007, pp. 489–492.

[31] A. Grau, J. Romeu, S. Blanch, L. Jofre, and F. De Flaviis, "Optimization of linear multielement antennas for selection combining by means of a butler matrix in different mimo environments," *Antennas and Propagation, IEEE Transactions on*, vol. 54, no. 11, pp. 3251–3264, 2006.

[32] A. Grau, J. Romeu, S. Blanch, L. Jofre, H. Jafarkhani, and F. De Flaviis, "Performance enhancement of the alamouti diversity scheme using polarization-reconfigurable antennas in different fading environments," in *Antennas and Propagation Society International Symposium 2006, IEEE*, 2006, pp. 133–136.

[33] B. Cetiner, L. Jofre, J. Y. Qian, and F. De Flaviis, "Small-size broadband multi-element antenna for rf/wireless systems," *Antennas and Wireless Propagation Letters, IEEE*, vol. 2, no. 1, pp. 326–329, 2003.

[34] L. Jofre, B. Cetiner, and F. De Flaviis, "Miniature multi-element antenna for wireless communications," *Antennas and Propagation, IEEE Transactions on*, vol. 50, no. 5, pp. 658–669, 2002.

[35] B. Cetiner, L. Jofre, and F. De Flaviis, "Reconfigurable miniature multielement antenna for wireless networking," in *Radio and Wireless Conference, 2001. RAWCON 2001. IEEE*, 2001, pp. 203–206.

[36] A. Grau, J. Romeu, L. Jofre, and F. de Flaviis, "Back-to-back high-isolation iso-frequency repeater antenna using mems-reconfigurable-parasitics," in *Antennas and Propagation Society International Symposium, 2007 IEEE*, 2007, pp. 497–500.

[37] J. De Luis, A. Besoli, J. Romeu, L. Jofre, and F. De Flaviis, "Bandwidth enhancement of high-isolation iso-frequency repeaters using mems-reconfigurable loaded parasitics," in *Antennas and Propagation Society International Symposium, 2008. AP-S 2008. IEEE*, 2008, pp. 1–4.

[38] E. Erdil, K. Topalli, M. Unlu, O. Civi, and T. Akin, "Frequency tunable microstrip patch antenna using rf mems technology," *Antennas and Propagation, IEEE Transactions on*, vol. 55, no. 4, pp. 1193–1196, 2007.

[39] J. Bernhard, E. Kiely, and G. Washington, "A smart mechanically actuated two-layer electromagnetically coupled microstrip antenna with variable frequency, bandwidth, and antenna gain," *Antennas and Propagation, IEEE Transactions on*, vol. 49, no. 4, pp. 597–601, 2001.

[40] D. H. W. Randy L. Haupt, *Genetic algorithms in electromagnetic*, I. John Wiley & Sons, Ed., 2007.

[41] E. Gopi, *Algorithm collections for digital signal processing applications using matlab*, Springer, Ed. National institute of technology, tiruchi, India, 2007.

[42] J. Robinson and Y. Rahmat-Samii, "Particle swarm optimization in electromagnetics," *Antennas and Propagation, IEEE Transactions on*, vol. 52, no. 2, pp. 397–407, 2004.

[43] G. Ciuprina, D. Ioan, and I. Munteanu, "Use of intelligent-particle swarm optimization in electromagnetics," *Magnetics, IEEE Transactions on*, vol. 38, no. 2, pp. 1037–1040, 2002.

[44] J. R. A. G. Franco De Flaviis, Lluis Jofre, *Multiantenna Systems for MIMO Communications (Synthesis Lectures on Antennas)*. Morgan and Claypool Publishers; 1 edition, 2006.

[45] J. R. J. R. S. B. A. Cardama, L. Jofre, *Antenas*, Alfaomega, Ed. Edicions UPC, 1999.

[46] C. Balanis, *Antena Theory: Analysis and Design*, I. Jhon Wiley & Sons, Ed., 1997.

[47] D. Paris, J. Leach, W., and E. Joy, "Basic theory of probe-compensated near-field measurements," *Antennas and Propagation, IEEE Transactions on*, vol. 26, no. 3, pp. 373–379, 1978.

[48] J. A. Stratton, *Electromagnetic Theory.* New York: McGraw-Hill, 1941.

[49] A. P. A.W Rudge, K.Milne, *The handbook of antenna design, Vol. 1*, I. E. waves series, Ed., 1982.

[50] E. B. J. Jofre, L. and R. Wilson, "Antenna pattern correction for range reflections," *Proc. Antenna Measurement Techniques Assoc. Symp.*, pp. 1 –6, 1987.

[51] E. Joy, J. Leach, W., and G. Rodrigue, "Applications of probe-compensated near-field measurements," *Antennas and Propagation, IEEE Transactions on*, vol. 26, no. 3, pp. 379–389, 1978.

[52] A. Yaghjian, "Efficient computation of antenna coupling and fields within the near-field region," *Antennas and Propagation, IEEE Transactions on*, vol. 30, no. 1, pp. 113–128, 1982.

[53] A. Besoli and F. De Flaviis, "A multifunctional reconfigurable pixeled antenna using mems technology on printed circuit board," *Antennas and Propagation, IEEE Transactions on*, vol. 59, no. 12, pp. 4413–4424, 2011.

[54] A. Grau and F. De Flaviis, "A distributed antenna tuning unit using a frequency reconfigurable pixel-antenna," in *Antennas and Propagation (EuCAP), 2010 Proceedings of the Fourth European Conference on*, 2010, pp. 1–5.

[55] D. Rodrigo, Y. Damgaci, N. Biyikli, B. Cetiner, J. Romeu, and L. Jofre, "Mems-reconfigurable antenna based on a multi-size pixelled geometry," in *Antennas and Propagation (EuCAP), 2010 Proceedings of the Fourth European Conference on*, 2010, pp. 1–4.

[56] R. Mehmood and J. Wallace, "Exploring beamforming performance versus complexity in reconfigurable aperture antennas," in *Smart Antennas (WSA), 2010 International ITG Workshop on*, 2010, pp. 383–389.

[57] D. Rodrigo, Y. Damgaci, M. Unlu, B. Cetiner, J. Romeu, and L. Jofre, "Antenna reconfigurability based on a novel parasitic pixel layer," in *Antennas and Propagation (EUCAP), Proceedings of the 5th European Conference on*, 2011, pp. 3497–3500.